SEDIMENTOLOGY the journal of the International Association of Sedimentologists IAS

Sedimentology (2024) doi: 10.1111/sed.13161

Radiocarbon ages of microcrystalline authigenic carbonate in Lake Neusiedl (Austria) suggest millennial-scale growth of Mg-calcite and protodolomite

STEPHANIE NEUHUBER*, SUSANNE GIER†, ERICH DRAGANITS†, PETER STEIER‡, MONIKA BOLKA‡, FRANZ OTTNER*, CHRISTOPH SPÖTL§, DOROTHEE HIPPLER¶ and PATRICK MEISTER†

**Institute of Applied Geology, University of Natural Resources and Life Sciences, BOKU, Peter Jordan Straße 82, Vienna 1190, Austria (E-mail: stephanie.neuhuber@boku.ac.at)*

†Department of Geology, University of Vienna, Josef-Holaubek-Platz 2, Vienna 1090, Austria (E-mail: patrick.meister@univie.ac.at)

‡Institute of Nuclear Physics (VERA), University of Vienna, Währingerstrasse 17, Vienna 1090, Austria

§Institute of Geology, University of Innsbruck, Innrain 52F, Innsbruck 6020, Austria

¶Institute of Applied Geosciences (IAG), Graz University of Technology, Rechbauerstraße 12, Graz 8010, Austria

Associate Editor – Andrea Martín Pérez

ABSTRACT

Authigenic Mg-calcite and dolomite are frequently observed in restricted, evaporative environments, such as lagoon or lake systems, but their formation is difficult to capture due to slow growth rates. Lake Neusiedl, an alkaline and subhaline lake with a mean water depth of 0.7 m in Austria, offers a natural system to study the precipitation of Ca-Mg-carbonate phases, which occur as fine-grained, unconsolidated and largely homogenized mud. To elucidate the timing and formation mechanisms of these authigenic carbonate phases, the mineralogical and isotopic composition and radiocarbon age of different sediment grain-size fractions from <0.2 to >3.0 μm were analysed. X-ray diffraction analyses show two broad peaks of Mg-calcite and protodolomite (lacking ordering peaks), suggesting that the carbonates are authigenic rather than detrital in origin. Calibrated carbon-14 ages range between 200 cal yr BP and 3700 cal yr BP. The linear correlation of age and grain size suggests a very slow growth rate of single crystals of 0.23 to 0.60 μm/ka. These rates suggest an extremely slow sedimentation rate in a shallow lake that existed during most of the Holocene. The higher abundance of protodolomite in older grain fractions, in contrast to the presence of high-Mg calcite in the youngest fractions, suggests a growth succession where high-Mg calcite develops first and subsequently transforms into protodolomite. Much higher ages of 6 cal ka BP to 15 cal ka BP are measured in carbonates of lake deposits exposed on land, in a section north-west of the recent lake, suggesting a growth rate of those carbonate minerals of 0.13 μm/ka. These time constraints further suggest that some carbonate grains could already have nucleated from lake water before or during the last glacial maximum, although under slightly different hydrochemical conditions.

Keywords Authigenic carbonate, Lake Neusiedl, Mg-calcite, protodolomite, radiocarbon age, stable carbon isotopes.

INTRODUCTION

Calcium–magnesium carbonates precipitated from oversaturated solutions in aquatic environments, so-called authigenic carbonates, represent a significant part of Earth's sedimentary record. Showing distinct mineralogical and geochemical signatures, they can serve as archives of past environmental conditions (e.g. Hardie, 1987; Viehmann *et al.*, 2020). Calcium–magnesium carbonates often form in evaporative marine and lacustrine environments, where they exhibit a diverse mineralogy, including hydrous, amorphous to poorly crystalline carbonates, aragonite, calcite and dolomite (e.g. Eugster & Hardie, 1978; Warren, 1990, 2010; Teal *et al.*, 2000; Gierlowski-Kordesch, 2010, and references therein). Calcite often shows a variable Mg-content, ranging from low-Mg calcite (LMC) to high-Mg calcite (HMC) and 'very-high-Mg calcite' (Lumsden & Chimahusky, 1980). The latter is also termed protodolomite (PD) if it contains more than 36 mol% $MgCO_3$ (Graf & Goldsmith, 1956) but lacks structural ordering of the cations (Machel, 2004; Gregg *et al.*, 2015) (an alternative definition of PD, i.e. showing partial cation ordering, was suggested by Gaines, 1977; this definition is not used here, since the apparent partial ordering essentially reflects a mixture of two phases, Mg-calcite and dolomite; see discussion in Gregg *et al.*, 2015). Protodolomite and dolomite do not form directly in modern ocean water, but they are common in restricted coastal lakes and carbonate platforms (for example, Coorong lakes, Australia: Von der Borch *et al.*, 1975; Warren, 1990; Lagoa Vermelha, Brazil: Vasconcelos *et al.*, 1995; coastal sabkhas of Abu Dhabi and Qatar: McKenzie, 1981; Wenk *et al.*, 1993; Bontognali *et al.*, 2010) or endorheic, saline and alkaline lakes (summarized by Last, 1990, and Last *et al.*, 2012), including Lake Nawar (Pakistan; Förstner, 1973a,b), Manito Lake (Canada; Last *et al.*, 2010), Deep Springs Lake (California; Peterson *et al.*, 1963; Clayton *et al.*, 1968; Meister *et al.*, 2011a,b), Lake Acigöl (Turkey; Balci *et al.*, 2016) and Lake Van (Turkey; McCormack *et al.*, 2018). However, the understanding of authigenic Ca-Mg-carbonate formation is incomplete in terms of mechanisms, rates and controlling factors, which limits its interpretation in the geological record.

For several of the examples cited above, it has been suggested that precipitation is penecontemporaneous, i.e. related to the evaporating surface water bodies (e.g. Meister *et al.*, 2011a,b; McCormack *et al.*, 2018; Fussmann *et al.*, 2020; Fang *et al.*, 2023), and this has also been proposed for some shallow-marine (Preto *et al.*, 2015; Meister & Frisia, 2019; Rieder *et al.*, 2019) and lacustrine dolomite occurrences (e.g. Reinhardt & Ricken, 2000; Hofbauer *et al.*, 2021) in the geological record. However, the formation of authigenic Ca-Mg-carbonates in modern aquatic environments is difficult to capture in real time. This is due to several circumstances: (i) The water chemistry and saturation state in evaporative environments is highly variable over short periods of time. (ii) The kinetics of Ca-Mg carbonate precipitation are poorly understood, and dolomite formation is known to be inhibited by a strong kinetic barrier (e.g. Land, 1998). Dolomite is presumably formed via ripening over extended periods of time (Land, 1998) and its formation thus cannot be monitored in real time. (iii) Authigenic, fine-grained mud particles become easily re-suspended by wave action and are difficult to discern from freshly formed crystals.

Ripening is an established concept based on the idea that minerals form in the sequence from metastable to more stable phases because metastable phases have lower kinetic barriers (Ostwald's step rule; Ostwald, 1897; Nordeng & Sibley, 1994; Sibley *et al.*, 1994). Following this concept, Deelman (1999) suggested that ripening occurs when the parent fluid fluctuates between super- and undersaturation with respect to a metastable precursor, while remaining supersaturated with respect to a stable phase. Laboratory studies found that, at high supersaturation, Ca-Mg-carbonate phases grow via ripening from an amorphous metastable phase and their transformation to a first crystalline phase occurs within hours to days (Rodriguez-Blanco *et al.*, 2012; Zhang *et al.*, 2012; Purgstaller *et al.*, 2016; Blue *et al.*, 2017). Subsequent reaction steps including recrystallization via dissolution–reprecipitation are much harder to capture in laboratory experiments because growth rates are often slow (Land, 1998; Rodriguez-Blanco *et al.*, 2012). Nucleation and successive ripening of Ca-Mg carbonates are moreover subject to several influences besides supersaturation, such as pH, cation ratios, ionic strength and presence of organic substances in the ambient fluid, that potentially affect the kinetic barrier of precipitation (Meister & Frisia, 2019; Meister *et al.*, 2023), and thereby modify element partitioning, mineralogical structure and rates of precipitation.

To advance understanding of authigenic carbonate formation in general and of PD in

particular, it is vital to disentangle the different steps of crystallization and potential growth pathways. For this reason, resolving the timing of Ca-Mg-carbonate nucleation and ripening in natural environments is of great importance for the understanding of these longer-term processes. In the 1960s, Peterson *et al.* (1963) performed a pioneering ^{14}C dating study of dolomite in Deep Springs Lake (California) using a sequential leaching method. The different fractions revealed increasing ages from the margin to the centre of micrometre-sized, zoned crystals, suggesting very slow growth rates in the order of tens of nanometres per thousand years, consistent with the above-mentioned predictions based on laboratory experiments.

In contrast to Deep Springs Lake, where dolomite shows an advanced degree of cation ordering, Lake Neusiedl, a shallow, subhaline lake in Austria, contains up to 70 cm of unconsolidated, fine-grained mud of Holocene age consisting of Ca-Mg carbonates with varying Mg content, including PD (Wieden, 1959; Schroll & Wieden, 1960; Müller *et al.*, 1972; Blohm, 1974; Löffler, 1979; Preisinger, 1979; Fussmann *et al.*, 2020) showing nanometre-scale domains of ordered dolomite (Meister *et al.*, 2023). In contrast to the hypersaline lakes mentioned above, Lake Neusiedl has a low salinity (1.0 to 2.5 g/l; Knie, 1959; Wolfram *et al.*, 2021; Appendix S1, Fig. S1), the lowest salinity of any lake with authigenic (proto)dolomite worldwide (Last, 1990), although higher values were reported from periods of high evaporation (up to 16 g/l in the 1930s; Auer & Dick, 1994). Hence, this system is suitable for studying the active formation of Mg-calcite precursors and their ripening to ordered dolomite.

The goal of this study was to constrain the timing and pathways of authigenic carbonate formation by radiocarbon dating in combination with mineralogical as well as stable C-isotope and O-isotope analyses. Radiocarbon dating of very small sample volumes of grain-size fractions from <0.2 to >3.0 μm provides apparent growth rates for different authigenic calcite phases of different stoichiometries. The reasoning is that larger crystals grew over a longer time compared to smaller ones, and thus different time sequences are integrated and preserved in different grain sizes. Therefore, grain-size separation of bulk sediment can provide insight into the temporal evolution of these lacustrine carbonates, because smaller grains will have formed over a shorter time span while larger ones had more time to grow. The main objective of this study was to confirm such a temporal relationship by dating Ca-Mg carbonates precipitated in this lake that could serve as a model system to better understand lacustrine and restricted marine carbonate deposits of the geological record.

STUDY AREA

Location and geological setting

Lake Neusiedl (German: Neusiedler See, Hungarian: *Fertő-tó*) is located at the border of Austria and Hungary. Due to its habitats and ecological significance, part of this area is a transnational National Park since 1993, a UNESCO World Heritage Site since 2001, and part of the European Union Natura 2000 network of protected environments since 2013. The lake is situated in the westernmost part of the Little Hungarian Plain or Danube Basin (Hungarian: *Kisalföld*), which is characterized by a very low relief and dominated by Quaternary fluvial and lacustrine sediments deposited on top of Pannonian (Upper Miocene) brackish and freshwater sediments (Fuchs & Schreiber, 1985). The area is located at the geodynamically and geomorphologically important intersection between the Alps, the Carpathians and the Pannonian Basin, and represents a complex deformation zone, which has been active since at least the Early Miocene (Székely *et al.*, 2009). High-resolution lake seismic surveys indicate very thin Pleistocene/Holocene lake sediments on top of Pannonian deposits that are slightly tilted towards the south-east along north-east/south-west trending strike-slip and normal faults (Loisl *et al.*, 2017; Zámolyi *et al.*, 2017). The larger area tilts towards the east, towards the subsidence centre of the Danube Basin at Győr (Šujan *et al.*, 2021), south-east of Lake Neusiedl. This tectonic movement was ongoing during the Quaternary, as indicated by the increase in Quaternary sediment thickness from almost zero at the lake to more than 25 m at the boundary between Austria and Hungary (Tauber, 1959; Häusler *et al.*, 2021a,b).

Hydrology

At present, the mean water level of Lake Neusiedl is located at 115.50 m above sea level (a.s.l.; at Trieste, Adriatic Sea) and the water body covers 321 km^2 (143 km^2 open water, 178 km^2 reed area;

Bácsatyai *et al.*, 1997). Despite its large surface area, its water depth is only about 1.4 m on average (Heine *et al.*, 2014) with a maximum depth of 1.8 m. The lake area and the wetlands to the east, including diverse saline ponds ('Seewinkel'), represent a highly dynamic system where the present-day extent of the water body and tributaries is very different from past conditions (Draganits *et al.*, 2022). At present, the catchment comprises 1120 km^2 (Herzig, 2014) and only the river Wulka and a few very small tributaries in the west and south of the lake provide surface water inflow (e.g. Soja *et al.*, 2013). Since the onset of instrumental measurement, the water balance is dominated by evaporation over precipitation, compensated by river inflow; the artificial canal is controlled by a sluice. For the period of 1967 to 1984, Reitinger *et al.* (1991) states an average of 184 Mm^3/year precipitation, 208 Mm^3/year evaporation, 47 Mm^3/year river inflow and 25 Mm^3/year outflow through the canal. Similar proportions were reported by Sailer & Maracek (2019) during the period of 1965 to 2018. The excess evaporation occurs mostly during the summer months, when the salinity increases, but also varies over several years (Federal Environmental Agency; Fig. S1 in Appendix S1). Such variable conditions may also have prevailed in historical times (several events are reported when the lake dried up completely) and probably during most of the prehistoric period. Episodically, at high water level, drainage occurs through the *Einser Kanal* (Sailer & Maracek, 2019), an artificial outlet finished in 1910 (Fally & Kárpáti, 2012), which connects the lake via the river Répce/Rabnitz with the Danube (Fig. 1). The lake water level is artificially kept at 115.50 m a.s.l. by closing the lake off via a weir at low water levels but draining it during episodes of high-water levels.

The present hydrology of Lake Neusiedl is very different from that in the past, as shown by historical maps, sediment data and geomorphological observations (Draganits *et al.*, 2007, 2008, 2022). The major reason for this drastic change is melioration by drainage channels and dams, from the 16th century onward (Draganits & Gmasz, 2023). Anthropogenic changes include the construction of a road dam between Fertőd and Pamhagen (completed in 1780), which progressively disconnected the lake from important tributaries including the Ikva, Répce/Rabnitz and Kis-Rába rivers. Still, during a flood of the Rába river in 1853, Lake Neusiedl was filled by these rivers from the south up to 117.60 m a.s.l. (Kovács, 2010). Before construction of the road dam, Lake Neusiedl and the Hanság area to the east formed a continuous wetland area with a catchment of approximately 8300 km^2 as opposed to 1120 km^2 today (Draganits *et al.*, 2022). Historical maps and sediment data as well as palaeo-shorelines indicate episodic lake levels up to 2 m above the present-day level (Draganits *et al.*, 2007), which is also consistent with the originally much larger catchment. However, drier periods with lower lake levels compared to today are also reported, for example, the lake fell largely dry from 1865 to 1870 (Moser, 1866; Sauerzopf, 1959) and possibly several times before (Sauerzopf, 1959; Kromp-Kolb *et al.*, 2005).

Holocene sediment infill and stratigraphy

The present lake is filled with unconsolidated sediment up to 0.7 m thick (Heine *et al.*, 2016, fig. 13), consisting mainly of HMC and PD, as documented by several studies since the 1950s (Wieden, 1959; and references cited above). The sediment thickness, however, varies strongly in different areas of the lake, with hardly any sediment in the north-east and an increase towards the south-west (Heine *et al.*, 2016). This heterogeneous distribution is largely due to resuspension and transport of the fine-grained unconsolidated sediment, since even moderate wind can generate currents and waves that mobilize sediment from the shallow lake bottom. Up to 1.10 m difference in lake level has been recorded at opposing shorelines as a result of this wind effect. ^{210}Pb dating of sediment cores documented recent sediment accumulation on the western shore, while no recent deposition was observed in the centre and along the eastern shore of the lake (Irlweck *et al.*, 1990). This study stated that no reliable sediment accumulation rate could be determined given the constant re-mobilization by wind as well as by erosion by ice in winter. Cores taken in Rust Bay on the western shore of the lake revealed a homogenous layer of 20 cm thickness, underlain by darker laminated sediment (Fussmann *et al.*, 2020). Thus, sediment accumulation following stratigraphic superposition is not expected in the upper homogeneous zone due to constant reworking. However, the laminated sediments pre-date the homogenous layer and record different sediment accumulation dynamics.

Near the village of Jois in the north-west of the lake, a lithostratigraphic section of older lake deposits shows more than 2 m of silty carbonate

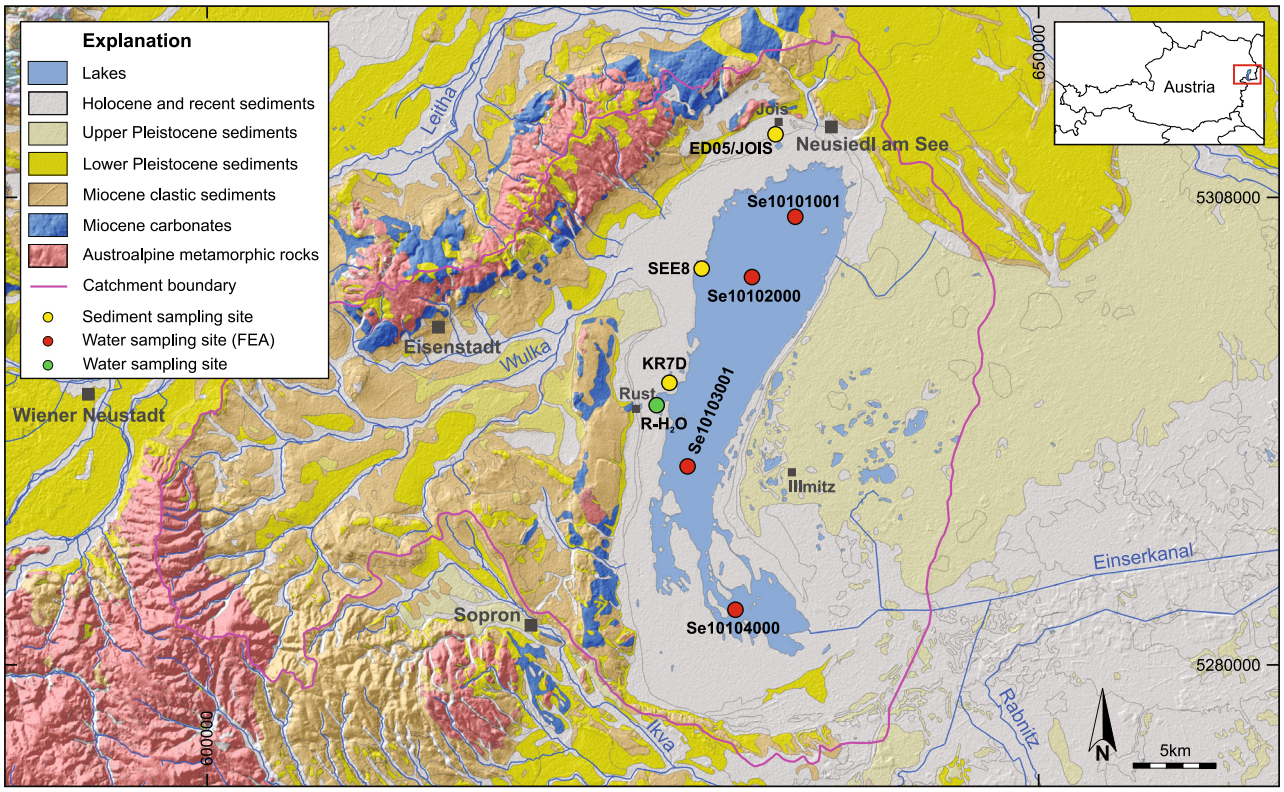

Fig. 1. Geological map of Lake Neusiedl (modified after Pascher *et al.*, 1999) with its main tributary (Wulka River), outlet (Einserkanal), and this study's sampling points for water (red and green dots) and sediment (yellow dots). Federal Environmental Agency.

mud covered by a chernozem soil (Draganits *et al.*, 2022, fig. 13.3). A shell fragment from the lower part of the profile yielded 14 439 ±223 cal yr BP. Such a thick carbonate succession is unknown from the modern lake.

Lake and porewater chemistry

The water composition of Lake Neusiedl is monitored several times per year by the Federal Environmental Agency (Umweltbundesamt, Vienna, Austria) at the stations shown in Fig. 1. The lake chemistry shows high ionic concentrations in comparison to other temperate freshwater lakes but low concentrations in comparison to most evaporative lakes. Its long-term average content of total dissolved solids is 1.0 to 2.5 g/l (Knie, 1959; Federal Environment Agency Austria, online database, 2000–2021; Wolfram *et al.*, 2021; see Appendix S1, Figs S1 and S2). The concentrations vary seasonally but also in the course of several years. Sodium concentrations in the range of 8 to 24 mmol/l have been recorded since 2000. In summer, concentrations are on average about 6 mmol/l higher than in winter, but larger variations occur over several years (Federal Environmental Agency; see Wolfram *et al.*, 2021, and compilation in Fig. S1). The lake water pH ranges between 8.7 and 9.2 (Fig. S1) but also higher variations were reported. Other than most oligohaline lakes, Lake Neusiedl has a high Mg/Ca ratio with varying concentrations of Ca and Mg (Ca: 0.2 to 1.1 mmol/l; Mg: 3.5 to 7.5 mmol/l). These variations can be explained by evaporative concentration in summer, while decreasing concentrations of Ca may be due to seasonal precipitation of carbonates. The relatively high Na-related alkalinity helps to buffer the pH so that the lake water is near the tipping point to a dilute soda lake (Wolfram *et al.*, 2021; see discussion below).

The lake shows significant primary production of organic matter (Gunatilaka, 1990), in particular along its reed-covered western shore. Primary production mainly comprises green algae and diatoms (e.g. Padisák & Dokulil, 1994). Anaerobic degradation as reflected by elevated NH_4^+,

HS^- and CH_4 is an important early diagenetic process (Tanzberger, 2005; Loisl *et al.*, 2017; Fussmann *et al.*, 2020). Organic carbon remineralization results in a diffusive gradient of dissolved inorganic carbon (DIC) reaching 12 mmol/l at 5 cm depth in the Bay of Rust (Fussmann *et al.*, 2020). Although alkalinity generally increases in the sediment, the lower pH (7.5 to 8.8) within the sediment compared to the water column reduces the saturation state with respect to carbonates near the sediment–water interface. This is due to anaerobic respiration and fermentation processes, which lower the saturation state even further compared to the upper water column, as reported in studies by Blohm (1974) and Fussmann *et al.* (2020).

METHODS

Sampling and sample processing

Three samples were investigated in this study; two were taken from sediments in the modern lake (samples KR7-D and SEE8-1) and one in older lake sediments exposed in a construction pit at the northern shore, near the village of Jois (sample ED05/JOIS/3; Draganits *et al.*, 2022). At the two sites in the lake, KR7 (N 47°48′53.68″/E 016°42′19.42″) and SEE8 (N 47°52′27.97″/E 016°44′01.61″; Fig. 1), recent unconsolidated lake sediment was retrieved by boat using an acrylic glass corer that was pushed into the sediment. The cores were processed in the laboratory of the Biological Station Neusiedler See at Illmitz within a few hours after sampling. The sediment was pushed out of the tubes and sliced into sections. The top 25 cm of the cores consisted of light grey, homogeneous, very fine-grained and water-saturated sediment. The lower part between 25 cm and 50 cm consisted of very fine-grained sediment with a lower water content and showed a more adhesive consistency. The top 25 cm of the homogeneous sediment (*ca* 750 ml) of each core was separated and further processed.

Sampling site ED05/JOIS (N 47°57′14.1″/E 016°47′30.8″; Fig. 1) was temporarily accessible in a construction pit. Around 300 g of light grey sediment was taken with a trowel from the wall of a trench at a depth of 1.6 m below surface (i.e. 116 m a.s.l.; 0.6 m below the base of the soil) and *ca* 1.5 m above today's groundwater level (Sample ED05/JOIS/3; Draganits *et al.*, 2022).

Grain-size separation and granulometry

Previous studies of Lake Neusiedl sediment samples have demonstrated that grain-size separation effectively separates coarser detrital particles from smaller authigenic crystals (Wieden, 1959; Schroll & Wieden, 1960; Blohm, 1974; Preisinger, 1979). Therefore, a stepwise centrifugation protocol following Tanner & Jackson (1948) was developed to obtain the grain-size fractions <0.2 μm, 0.2 to 0.5 μm, 0.5 to 1.0 μm, 1 to 2 μm, 2 to 3 μm and >3 μm by extracting the smallest fraction first, followed by re-suspension and removal of the next coarser grain-size fraction. All grain-size separates were dried at 80°C. Afterwards, each fraction was split into aliquots, which were used for further analyses.

The grain-size distribution of two samples (SEE8-1 and KR7-D; Fig. S3) was determined using a SediGraph5100 (Micromeritics, Norcross, GA, USA) on 3 g bulk sample after drying at 80°C and re-suspension. Na-tripolyphosphate was used as a dispersant.

Thermogravimetry by simultaneous thermal analysis

Simultaneous thermal analysis (STA) measures the weight loss due to endothermic and exothermic reactions to identify organic and inorganic carbon phases. For each sample 50 mg, were heated to 1000°C in a Netzsch Simultaneous Thermal Analyser (STA 409PC LUXX®; Netzsch, Selb, Germany) with gas control (PU1.851.06) using a 50 ml/min air and 15 ml/min N_2 gas flux rate, and a temperature increase of 10°C/min. The amounts of organic and inorganic carbon were measured by weight loss. Results were quantified according to different reaction temperatures using the built-in software at the Institute of Applied Geology (University of Natural Resources and Life Sciences, Vienna, Austria). The analytical uncertainty is smaller than 2% of the measured value. The contributions of carbonate phases were calculated using the stoichiometric conversion factor for CO_2 loss from carbonates, which differs for calcite (2.274) and dolomite (2.095). Concentrations for pure calcite and pure dolomite stoichiometry were calculated, and the average of the two results is reported as carbonate content (Fig. 2). The total wt% of organic carbon and carbonate phases were subtracted from 100 wt% to obtain the weight-percentage of silicate phases.

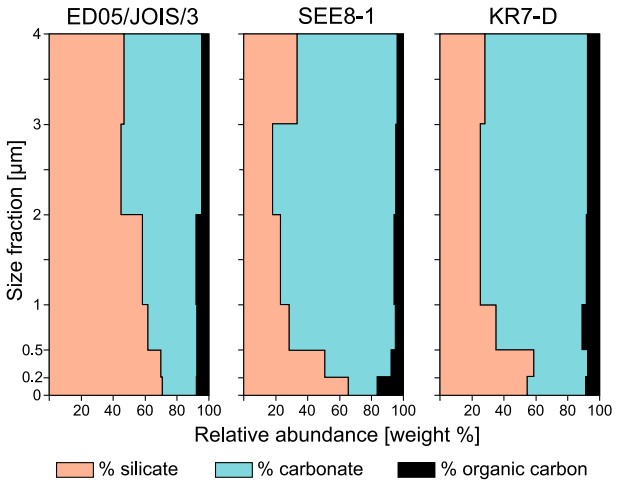

Fig. 2. Distribution of silicate, carbonate and organic carbon phases determined by simultaneous thermal analysis (STA) in the grain-size fractions of modern and ancient lake sediment samples. Locations arranged north to south from left to right.

Mineralogy and Mg content of carbonate minerals

Powder X-ray diffraction (XRD) (Panalytical PW 3040/60 X'Pert PRO, CuKα radiation, 40 kV, 40 mA, step size 0.0167° 2θ, 5 s per step; Malvern Panalytical Limited, Malvern, UK) was used on oriented and unoriented samples at the Department of Geology, University of Vienna (Austria) to identify the mineral phases present in the different size fractions. Quartz (107 536; Merck, Darmstadt, Germany) was used as an internal standard. For determination of the peak positions and quantification of peak areas of carbonate minerals the 'fit profile' option of the Panalytical X'Pert Highscore plus software was used. The extent of Mg substitution in calcite was calculated from the (104) peak shift according to the method of Goldsmith & Graf (1958).

Scanning electron microscopy

High-resolution secondary electron (SE) microscopy of selected sample fractions was performed using a Zeiss digital scanning electron microscope (SEM) (DSM 982 Gemini; Carl Zeiss AG, Oberkochen, Germany) equipped with a field emission gun, at the Institute of Earth Sciences at the University of Graz, Austria. For this purpose, 1 to 5 mg of sediment was loosely disseminated on SEM sample holders and coated with Au-Pd. Observations were made in SE mode in high vacuum (3.0^{-9} µPa) at an accelerating voltage of 2 kV and a probe current of 2350 mA.

Stable carbon and oxygen isotopes

Aliquots of different grain-size fractions were analysed in duplicate (and triplicate for sample KR7-D) for their stable carbon and oxygen isotope composition ($\delta^{13}C_{carb}$ and $\delta^{18}O_{carb}$) using a Thermo Fisher Delta^{Plus}XL mass spectrometer equipped with a GasBench II (Thermo Fisher Scientific, Bremen, Germany) at the Institute of Geology at the University of Innsbruck, Austria, following the procedure of Spötl & Vennemann (2003). Results were calibrated against calcite NBS 19, CO1 and CO8 reference materials and reported as ‰ relative to Vienna PeeDee Belemnite (VPDB). The long-term 1-sigma uncertainty of $\delta^{13}C$ and $\delta^{18}O$ values is ±0.06 and ±0.08‰, respectively.

Radiocarbon analyses

To test whether lake water CO_2 is equilibrated with CO_2 from the atmosphere, CO_2 was purged from 2 l of lake water with He and trapped in liquid N_2. A dissolved carbonate standard (40 pMC corresponding to 0.4 $F^{14}C$) was processed as a blank using the same setup. Trapped CO_2 was immediately graphitized for radiocarbon analysis.

In addition, radiocarbon was analysed on different grain-size fractions of each sample following the method described in Steier *et al.* (2017). In short, 50 µg of sample powder was hydrolysed in valve-sealed quartz vials by phosphoric acid at approximately 50°C for 1 h. The produced CO_2 was cryogenically purified and reduced to graphite using hydrogen and an Fe-catalyst (Bosch reaction). The ^{14}C content was quantified by accelerator mass spectrometry (AMS) at the Vienna Environmental Research Accelerator (VERA) at the Institute of Nuclear Physics, University of Vienna, Austria. Data are reported as $F^{14}C$, which is the ^{14}C content relative to a hypothetical 'modern' reference value, defined as 95% of the content of the NIST oxalic-I standard (Stuiver & Polach, 1977) and corrected for isotopic fractionation. The advantage of reporting $F^{14}C$ is that numbers obey simple equations in mixing processes, whereas calculated radiocarbon ages behave strongly nonlinearly and cannot be directly used in mixing equations. For calibration of radiocarbon ages, the program OxCal 4.4 (Bronk

Ramsey, 2009) with the IntCal20 calibration curve (Reimer *et al.*, 2020) was used.

RESULTS

Granulometry and mineral composition

Grain-size analyses of samples KR7-D and SEE8-1 exhibit similar grain-size distribution patterns, with 87% (weight/volume) in the <10 μm fraction and 42% in the <3 μm fraction (Fig. S3). According to STA analyses, carbonates contribute 18 to 79 wt%, organic carbon 3 to 16 wt%, and the remaining silicates 17 to 71 wt% to the different size fractions (Fig. 2; Table 1). In the fractions <1 μm, the abundance of carbonate minerals is generally lower and the abundance of silicate minerals higher than average (Fig. 2).

At all three locations, the sediment contains quartz, muscovite, Fe-chlorite, K-feldspar, plagioclase, LMC and PD (Fig. 3A). In modern lake sediments, a broad peak of HMC is present in XRD patterns (around 60%; Fig. 3A and B), but this phase is depleted in the >3 μm fractions. Most carbonates are depleted in the <0.5 μm fractions, where a broad peak appears instead.

The degree of Mg substitution in calcite allows identifying carbonate minerals of different Mg content (Figs 3 and 4; Table 2). In modern lake sediments, carbonate phases are dominated by a continuum with two broad peaks in the 2θ region between 29.5° and 31°. In most fractions, only minor amounts of poorly defined LMC (by definition, the LMC–HMC boundary is at 4 mol% $MgCO_3$; Tucker, 2001; Bischoff *et al.*, 1993) are indicated by a terrace in the HMC peak near 29.6° 2θ. Stoichiometric calcite (3.04 Å) and stoichiometric (proto)dolomite (2.88 Å) were only detected in the >3 μm fraction (Fig. 3B). Sample ED05/JOIS/3 shows predominantly (71 to 93%) a LMC–HMC cluster (1 to 7 mol% $MgCO_3$; here referred to as 'LMC') and low amounts of PD (7 to 29%; 43 to 49% $MgCO_3$) but lacks the broad HMC peak. In the <0.2 μm and >3.0 μm fractions, (proto)dolomite has a stoichiometric composition (*ca* 50 mol% $MgCO_3$).

The degree of dolomite ordering is indicated by the 015 : 110 peak ratio according to Füchtbauer & Goldschmidt (1966). However, only traces of the 015 peak could be identified in the bulk fractions (Fig. 3C) and show no systematic distribution in the different grain-size fractions. The peak may indicate incipient cation ordering (see details in Meister *et al.*, 2023), while the overall phase has predominantly a calcite structure, and hence is regarded as PD.

Scanning electron microscope (SEM) imaging of sample SEE8-1 reveals that a portion of the carbonate fraction forms rhombohedral to irregular crystals with diameters between 0.5 μm and 1.0 μm (Fig. 5A). Judging from their different shapes, several generations of crystals are present. Their surfaces reveal a high abundance of kinks (Fig. 5B).

Stable carbon and oxygen isotopes

The $\delta^{13}C$-values from modern lake sediments range between −3.8‰ and −2.2‰ in all fractions, with one outlier of 3.2‰ in the >3 μm fraction from site SEE8, while at site ED05/JOIS the values range from −1.7 to −0.1‰ (Fig. 6A and B; Table 1). Two size fractions from sample ED05/JOIS/3 (0.2 to 0.5 μm and 1 to 2 μm) scatter widely, presumably due to incomplete homogenization. $\delta^{13}C$-values decrease with increasing grain size. Only the fine fractions (<0.2 μm and 0.2 to 0.5 μm) deviate from this trend, showing mostly lower values (Fig. 6B).

The oxygen isotope values range from −3.6 to −0.4‰ with one outlier (KR7-D 0.2 to 0.5 μm: 9.2 ±0.4‰; Fig. 6A and C). A slight difference of 0.3 to 0.5‰ is observed between samples SEE8-1 and KR7-D, where all size fractions from sample SEE8-1 show lower values. In sample ED05/JOIS/3, all grain sizes show values that are largely within the range of the values of the modern lake sediment. Analogous to carbon isotopes, $\delta^{18}O$ values show a slight decreasing trend with increasing grain size and a deviation from this trend in the small grain-size fractions. Moreover, a covariant trend of $\delta^{13}C$ versus $\delta^{18}O$ values was revealed for the different size fractions of the samples SEE8-1 and KR7-D (Fig. 6A).

Radiocarbon activity

Carbon dioxide purged from lake water sampled on 1st March, 2017 (surface water at the pier of Rust harbour; for location see Fig. 1) yielded a modern radiocarbon activity ($F^{14}C$) of 1.04 ±0.02 (cf. 1.015 as the atmospheric value from 2017; Hua *et al.*, 2022), and documents that the lake water is equilibrated with the atmosphere.

Grain-size fractions of all samples yielded measurable radiocarbon contents (Table 1). Radiocarbon activities ($F^{14}C$) in sediments taken from within the lake range between 0.64 and 0.91 for sample SEE8-1, and between 0.76

Table 1. Stable carbon and oxygen isotope values, relative abundances of silicate, carbonate and organic carbon phases (from thermogravimetry), and radiocarbon data for grain-size separates of the locations SEE8, KR7-D and ED05/JOIS. Radiocarbon activity is reported as fraction of modern ^{14}C ($F^{14}C$) which is equivalent to percent modern carbon (pMC) divided by 100.

Sample	Grain size [μm]	$\delta^{13}C$ [‰ VPDB]	1σ	$\delta^{18}O$ [‰ VPDB]	1σ	Silicate [%]	Carbonate [%]	TOC [%]	$F^{14}C$	1σ	Age [BP]	1σ	Age (cal) [a BP]	1σ	Age (corr, cal) [a BP]	1σ
SEE8-1	>3*	3.21	0.06	−2.86	0.01	33	64	3	0.641	0.005	3676	89	3869	95	3768	86
SEE8-1	2–3*	−2.70	0.03	−2.10	0.01	17	79	4	0.833	0.006	1510	69	1364	53	839	57
SEE8-1	1–2*	−2.57	0.05	−2.54	0.01	22	73	5	0.865	0.006	1199	65	1082	75	667	47
SEE8-1	0.5–1	−2.73	0.04	−2.31	0.01	28	68	4	0.886	0.006	1001	62	935	58	605	46
SEE8-1	0.2–0.5*	−2.94	0.02	−3.55	0.01	51	42	7	0.905	0.006	825	60	726	48	318	110
SEE8-1	<0.2*	−2.22	0.05	−1.47	0.01	66	18	16	0.919	0.009	698	85	629	56	219	130
KR7-D	>3†	−2.90	0.06	−0.90	0.06	28	66	7	0.759	0.028	2280	313	2242	360	1573	327
KR7-D	2–3†	−2.85	0.03	−0.75	0.01	25	68	7								
KR7-D	1–2†	−2.68	0.05	−0.52	0.07	25	68	8	0.795	0.008	1896	95	1752	100	1189	86
KR7-D	0.5–1†	−2.84	0.04	−0.42	0.01	35	55	10	0.843	0.010	1412	107	1269	97	763	88
KR7-D	0.2–0.5†	−3.35	0.02	9.23	0.42	59	34	7	0.890	0.020	963	189	884	166	358	172
KR7-D	<0.2†	−3.82	0.05	−2.98	0.17	55	37	8	0.916	0.032	725	287	692	266	239	166
ED05/JOIS/3	>3*					47	49	4	0.200	0.000	13 305	296	15 457	315		
ED05/JOIS/3	2–3*	−0.39	–	−2.92	–	45	50	5	0.258	0.004	11 200	204	12 861	110	12 531	182
ED05/JOIS/3	1–2*	−0.10	1.05	−0.83	0.18	59	33	8	0.272	0.006	10 763	254	12 283	278	11 958	339
ED05/JOIS/3	0.5–1*	−0.06	0.07	−1.38	0.11	62	31	7	0.304	0.011	9843	361	10 938	435	10 575	403
ED05/JOIS/3	0.2–0.5*	−1.69	0.79	−2.22	1.13	70	23	8	0.419	0.006	7191	167	7818	105	7482	94
ED05/JOIS/3	0.2–0.5 rep.								0.488	0.006	5931	142	6565	113		
ED05/JOIS/3	<0.2					71	21	8	0.326	0.005	9266	190	10 094	191		
Lake Neusiedl, Water									1.04	0.02						

* Duplicate measurements for stable isotopes. † Triplicate measurements for stable isotopes.

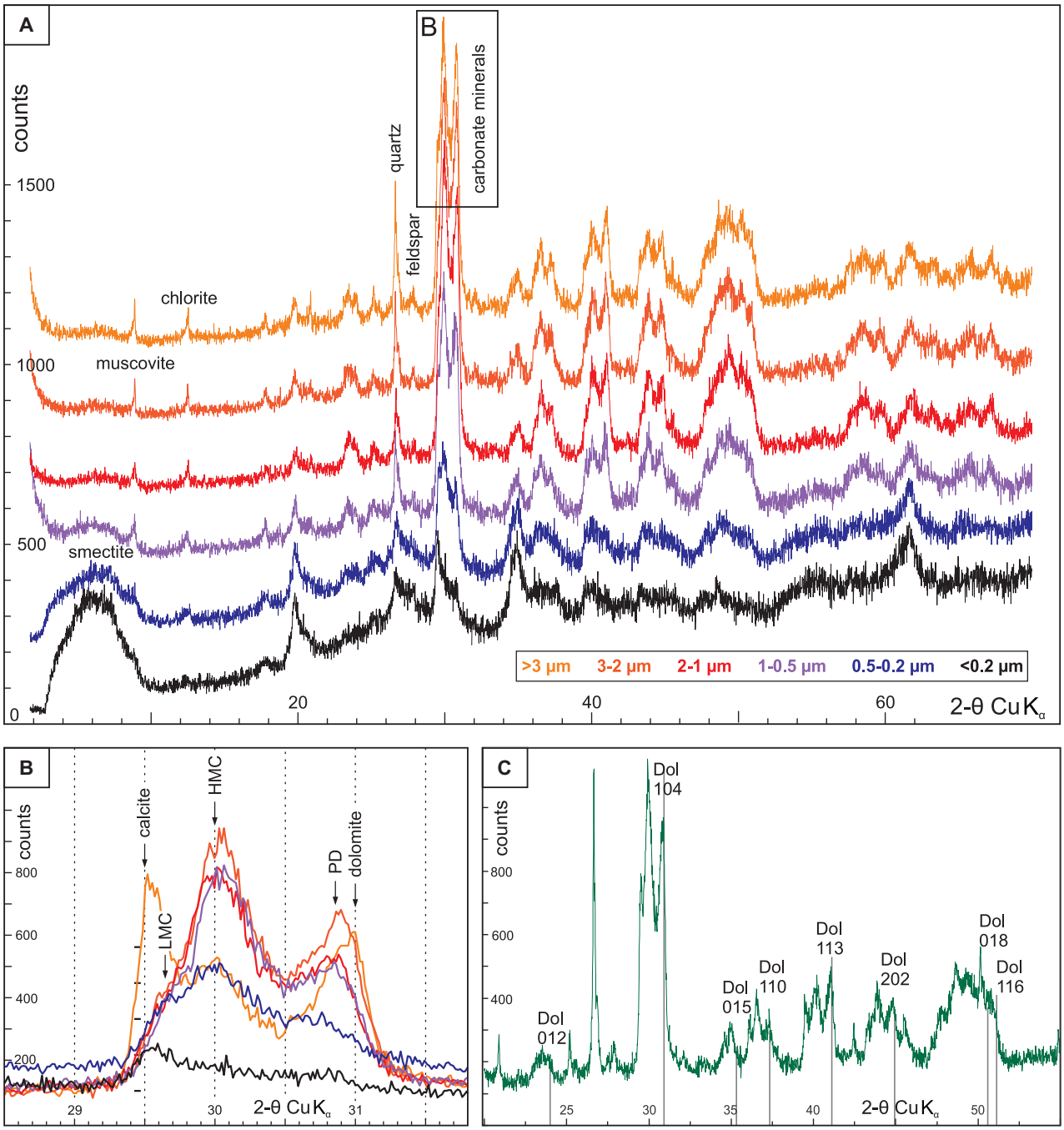

Fig. 3. (A) X-ray diffractograms of grain-size separates of sediment sample KR7-D. The patterns show the presence of muscovite, chlorite, quartz, feldspar, calcite and protodolomite, with a broad peak of high-Mg calcite (HMC) which decreases in the >3 µm fraction, while the peaks in the regions of low-Mg calcite (LMC) and dolomite/protodolomite increase. (B) Detailed view of the 2θ region with the 104 peaks of carbonate phases in different grain sizes. (C) Close-up of the 2θ range showing the 015 ordering peak of dolomite relative to the 110 peak. A small ordering peak is visible in the bulk sample.

and 0.92 for sample KR7-D (Fig. 7). Lower $F^{14}C$ values from 0.26 to 0.33 were measured in sample ED05/JOIS/3. The radiocarbon activity of sediment samples from all sites decreases with increasing grain size. All samples follow a linear trend of decreasing radiocarbon activity, except for the coarsest fraction which deviates from the trend by a higher depletion in ^{14}C content

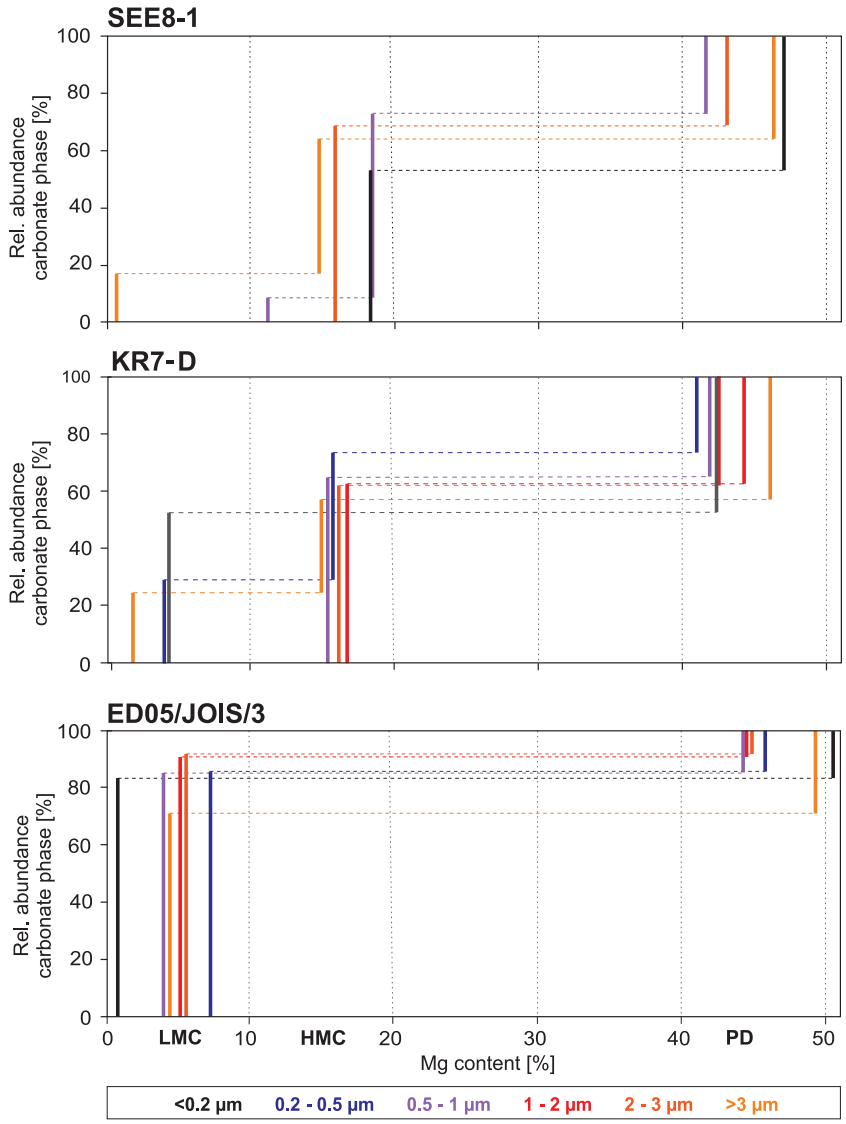

Fig. 4. Carbonate phase distribution of different grain-size fractions; position on the *x*-axis indicates Mg content (in mol%) of the carbonate minerals calculated from X-ray diffraction (XRD) measurements (Goldsmith & Graf, 1958). Lengths of each line on the *y*-axis add up to 100% for each carbonate phase and specify their relative abundance. The length of each line indicates the relative percentage of a phase in a particular grain-size fraction. HMC, high-Mg calcite; LMC, low Mg-calcite; PD, protodolomite.

(Table 1). Conventional (uncalibrated) radiocarbon ages range from 700 to 3700 BP increasing with grain size (see column '^{14}C age' in Table 1; Fig. 8A). Calibration and corrections will be discussed below.

The finest grained subsample of ED05/JOIS/3 (<0.2 μm) with the highest radiocarbon activity of all Jois subsamples ($F^{14}C = 0.33$) consists only of LMC and PD. Here, $F^{14}C$ decreases from 0.30 in the 0.5 to 1.0 μm fraction to 0.26 in the 2 to 3 μm fraction. One subsample from ED05/JOIS/3 (0.2 to 0.5 μm) was marked as an outlier (see discussion below) due to its scatter in both radiocarbon and stable isotope values. Conventional radiocarbon ages range from 6000 to 13 300 BP with increasing grain size (see column '^{14}C age' in Table 1; Fig. 8B).

DISCUSSION

Radiocarbon ages and timing of authigenic mineral formation

The measured radiocarbon activity depends primarily on the average age of carbon in the sediment grains, integrating the old nucleus and the younger rim. The derived radiocarbon age, and hence the timing of mineral precipitation, may be altered by the contribution of pre-aged carbon from other pools, for example, from organic matter, mixing of phases of different age, recrystallization, or variations in atmospheric radiocarbon activity through time. In the following, the different effects are assessed, and their magnitude estimated in order to reliably constrain

Table 2. Mineralogical data extracted from X-ray diffraction (XRD) patterns for grain-size separates of the locations See SEE8, KR-7 and ED05/JOIS: d-values of 104 peaks of different calcite, and PD, phases and conversion of d-values into mol% Ca and Mg for each peak, according to the equation of Goldsmith & Graf (1958). Estimated relative abundances are based on the ratios of individual 104 peak areas to the summed 104 peak areas.

		LMC				HMC				PD			
Sample	Grain size [μm]	d value	mol% Mg*	mol% Ca	% area	d value	mol% Mg	mol% Ca	% area	d value	mol% Mg	mol% Ca	% area
SEE8-1	>3	3.029	1	49	17	2.988	15	35	47	2.896	47	3	36
SEE8-1	2–3					2.982	16	34	68	2.906	43	7	32
SEE8-1	0.2–0.5	3.010	11	39	9	2.976	19	31	64	2.909	42	8	27
SEE8-1	<0.2	3.019				2.979	18	32	78	2.897	47	3	22
KR7-D	>3	3.027	2	48	24	2.985	15	35	33	2.896	46	4	43
KR7-D	2–3					2.983	16	34	62	2.906	43	7	38
KR7-D	1–2					2.981	17	33	63	2.901	44	6	37
KR7-D	0.5–1					2.985	16	34	65	2.908	42	8	35
KR7-D	0.2–0.5	3.020	4	46	29	2.983	16	34	44	2.910	41	9	27
KR7-D	<0.2	3.019	4	46	53					2.907	42	8	47
ED05/JOIS/3	>3	3.019	ts	46	71					2.888	49	1	29
ED05/JOIS/3	2–3	3.016	5	45	93					2.900	45	5	7
ED05/JOIS/3	1–2	3.016	5	45	92					2.901	45	5	8
ED05/JOIS/3	0.5–1	3.018	4	46	85					2.902	44	6	15
ED05/JOIS/3	0.2–0.5	3.012	7	43	85					2.899	45	5	15
ED05/JOIS/3	<0.2	3.031	1	49	83					2.888	50	0	17

* Calcite with more than 4% Mg would be by definition HMC, but here it clusters with LMC.

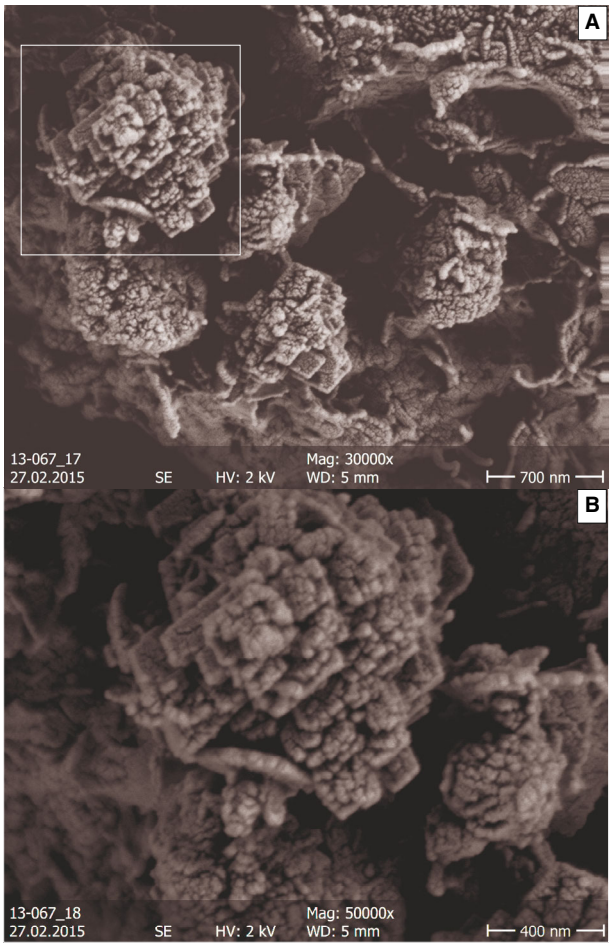

Fig. 5. Scanning electron microscopy (SEM) photomicrographs showing the shape and size of Ca-Mg carbonate crystals in sample SEE8-1. (A) Overview shows several grains in the order of 0.5 to 1.0 μm. The overall shapes tend to be round to rhombohedral while their surfaces always are nano-facetted. (B) Close-up of the area in the white frame in (A) showing that the facets of the grain are largely in crystallographic continuity. Presumably, the different grain types represent different generations of crystal phases.

the ages for the different authigenic carbonate phases.

Conversion of $F^{14}C$ into calendar ages

Radiocarbon ages can be calculated from $F^{14}C$ values using the formula of Libby *et al.* (1949), Arnold & Libby (1949) and Stuiver & Polach (1977) using the half-life of ^{14}C of 5730 ±40 years (Godwin, 1962). The resulting ages of 700 to 3700 BP for the modern lake sites and 6000 to 13 300 BP for site ED05/JOIS increase with grain size. These calculated ^{14}C ages do not account for atmospheric ^{14}C variations over time. This effect can be corrected by calibrating $F^{14}C$ values to the atmospheric ^{14}C curve (Reimer *et al.*, 2020). The calibrated ages (column 'Age cal' in Table 1 and displayed in Fig. 8) are only slightly different for younger ages in modern lake sediments, but the ages of the older samples from ED05/JOIS (ED05/JOIS/3, >3 μm; 15 457 cal yr BP) are shifted by more than 2000 years towards older ages.

Contribution of pre-aged carbon

When carbonate minerals precipitate from aqueous solutions, they can be assumed to be in isotopic equilibrium with the dissolved inorganic carbon (DIC) species. Kinetic fractionation of C and O isotopes during carbonate precipitation has been observed under extreme conditions (e.g. Meister *et al.*, 2011b) but is most likely insignificant in a lacustrine system, such as Lake Neusiedl. If DIC is solely of atmospheric origin, the timing of carbonate precipitation can be determined by the radiocarbon content of the mineral phases. However, dating of lacustrine carbonates is often limited by the effect that 'old' carbonate rocks are dissolved in the catchment, which provides ^{14}C-free DIC, diluting the ^{14}C activity of the sample and, thus, resulting in anomalously low radiocarbon activities (also known as 'hard water effect').

Radiocarbon measurements of CO_2 sparged from Lake Neusiedl water yielded a modern activity ($F^{14}C$ of 1.04, local variations up to the order of 0.04 are possible; Reimer *et al.*, 2004; Major *et al.*, 2018) which suggests full equilibration with atmospheric CO_2. In comparison, atmospheric $\delta^{13}C_{CO2}$ data from the nearby meteoric station at Hegyhatsal (46.97°N, 16.38°E, 240 m a.s.l.) vary between −7‰ and −10‰ (Demény & Haszpra, 2002), which matches well the modern $\delta^{13}C_{CO2}$ in the atmosphere, with some variations reflecting seasonal changes in CO_2 uptake (Troilier *et al.*, 1996). The large surface area and shallow water depth in combination with wind-driven waves and currents result in strong mixing of the lake water several times per year and may support equilibration of the lake's DIC pool with atmospheric CO_2. However, despite the measured atmospheric ^{14}C signature of the surface water, $\delta^{13}C$-values of the carbonates range between −3.8‰ and −2.2‰ in samples KR7-D and SEE8-1 in the modern lake sediments, which is several permille lower than values of calcite or dolomite that would form from DIC in equilibrium with atmospheric CO_2 (based on the fractionation factor by Mook

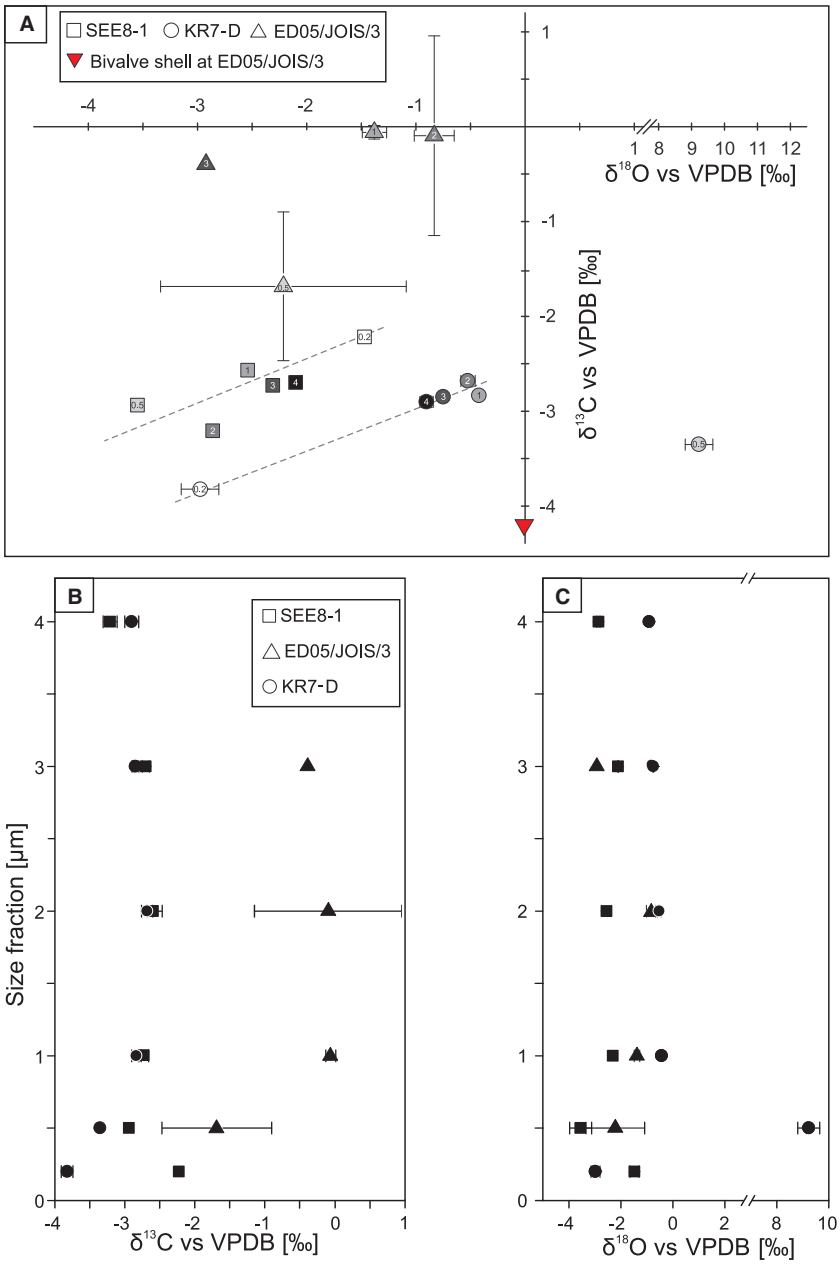

Fig. 6. (A) Stable carbon and oxygen isotope values of carbonate samples from Lake Neusiedl. The respective grain sizes are indicated by the level of grey shading and are labelled within each symbol. Error bars are 1 σ SD of duplicate measurements of the samples and are mostly within the size of the symbol. Dashed lines indicate the covariance between $\delta^{13}C$ and $\delta^{18}O$ values in the samples SEE8-1 and KR7-D. The value measured for a bivalve shell from site ED05/JOIS is indicated. (B) Stable carbon isotope composition and (C) oxygen isotope composition of different grain-size fractions for the three sampling sites.

et al., 1974, between CO_2 and bicarbonate). The isotopic composition of bicarbonate in equilibrium with this calcite and dolomite would range from −6.6 to −4.0‰ and from −8.3 to −6.7‰, respectively (according to the fractionation factor; see calculation in Appendix S1, Table S1). Since HCO_3^- is the most abundant species at a pH between 6 and 9, its isotopic composition should approximately represent the composition of the DIC, and indeed the $\delta^{13}C$-values calculated for HCO_3^- match well with $\delta^{13}C$-values between −5.6 and −2.0‰ in DIC of lake water measured in 2019 and 2020 (Schnedlitz, 2020). Sediments from the onshore site ED05/JOIS show less negative $\delta^{13}C$-values, but they are also more negative than they would be if they had formed in isotopic equilibrium with atmospheric CO_2.

Isotopically light DIC fixed during primary production in the surface water (Hollander & McKenzie, 1991) is released from degradation of organic matter (Botz & Von der Borch, 1984; Botz *et al.*, 1988). Primary production by C3 plants and algae results in biomass of

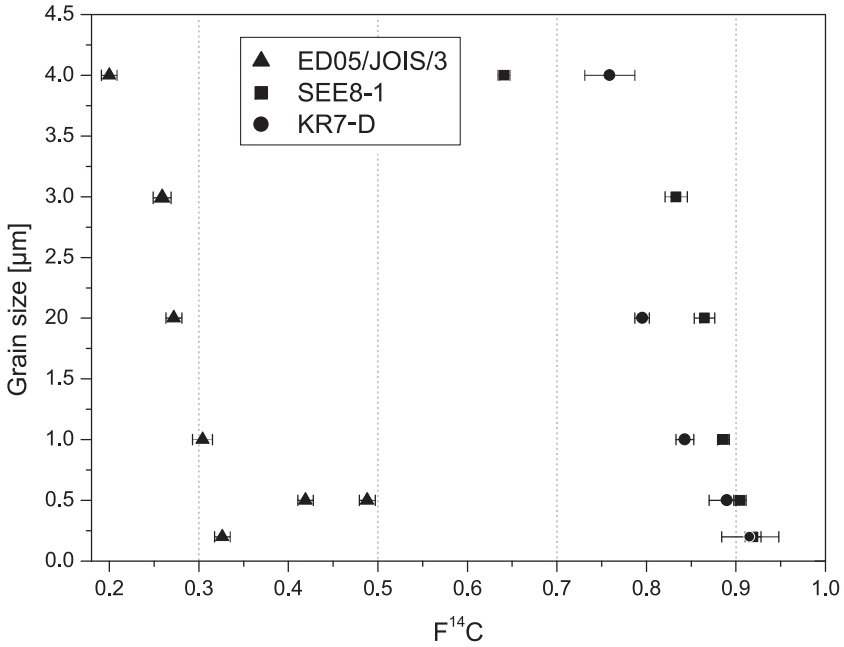

Fig. 7. Radiocarbon activity ($F^{14}C$) of the three samples SEE8-1, KR7-D and ED05/JOIS/3 in relation to grain size. The values largely show a linear decreasing trend with increasing grain size, but more depleted values in the >3 µm fraction. The values from sample ED05/JOIS/3 are much lower and do not overlap with the range observed in the modern lake sediment.

approximately −25‰, so that organic matter intermixed with the lake sediment can be expected to show similar values. Fussmann *et al.* (2020) demonstrated that organic matter is degraded by anaerobic dissimilatory metabolism in the lake sediment, linked to several electron acceptors (nitrate, ferric iron and sulphate), but also via aerobic respiration near the sediment–water interface. The release of inorganic carbon results in a downward increasing gradient, reaching 12 mmol/l DIC at 5 cm (18 mmol/l at 30 cm) below the sediment–water interface and further increasing below. Hence, DIC diffuses upward and across the sediment–water interface and becomes intermixed with lake water. Even more extreme fractionation may occur during methanogenesis, but this effect may become counterbalanced by ^{13}C-enriched CO_2, also produced during methanogenesis (Meister & Reyes, 2019). Somewhat less negative values would result from degrading *Phragmites* reeds, abundantly present on the western shore of the lake, which ranges between −10‰ and −18‰ (mean −13‰; O'Leary, 1981). Another potential source of isotopically light carbon is DIC from tributaries to Lake Neusiedl, in which Schnedlitz (2020) measured $\delta^{13}C$ values as low as −11‰, most likely derived from the degradation of organic matter from soil.

To test the effect of pre-aged DIC from organic matter degradation on $F^{14}C$ values and radiocarbon ages, a sensitivity test was performed, assuming a $\delta^{13}C_{TOC}$ of −25‰ and varying the age of total organic carbon (TOC; at the time of carbonate precipitation). Since $F^{14}C$ values are not affected by isotope fractionation, the atmospheric $F^{14}C$ and the $F^{14}C$ of pre-aged TOC can be mixed in the proportion indicated by the $\delta^{13}C$ mass balance (for the calculation see Appendix S1, Table S1). A pre-aged DIC pool, due to TOC input, would mean that the carbonate phases are in fact younger than indicated by the measured radiocarbon activity. Thus, a higher assumed age of TOC will result in younger ages for the carbonate phases. The TOC-age can be varied to the point where radiocarbon ages of carbonates are negative.

Note that the corrected ages also need to be calibrated for the change in atmospheric ^{14}C over time. This calibration can only be considered as a rough estimate, because multiple sources of C with different ages may have contributed to the overall ^{14}C activity of the carbonate phase, and each source would require its own calibration.

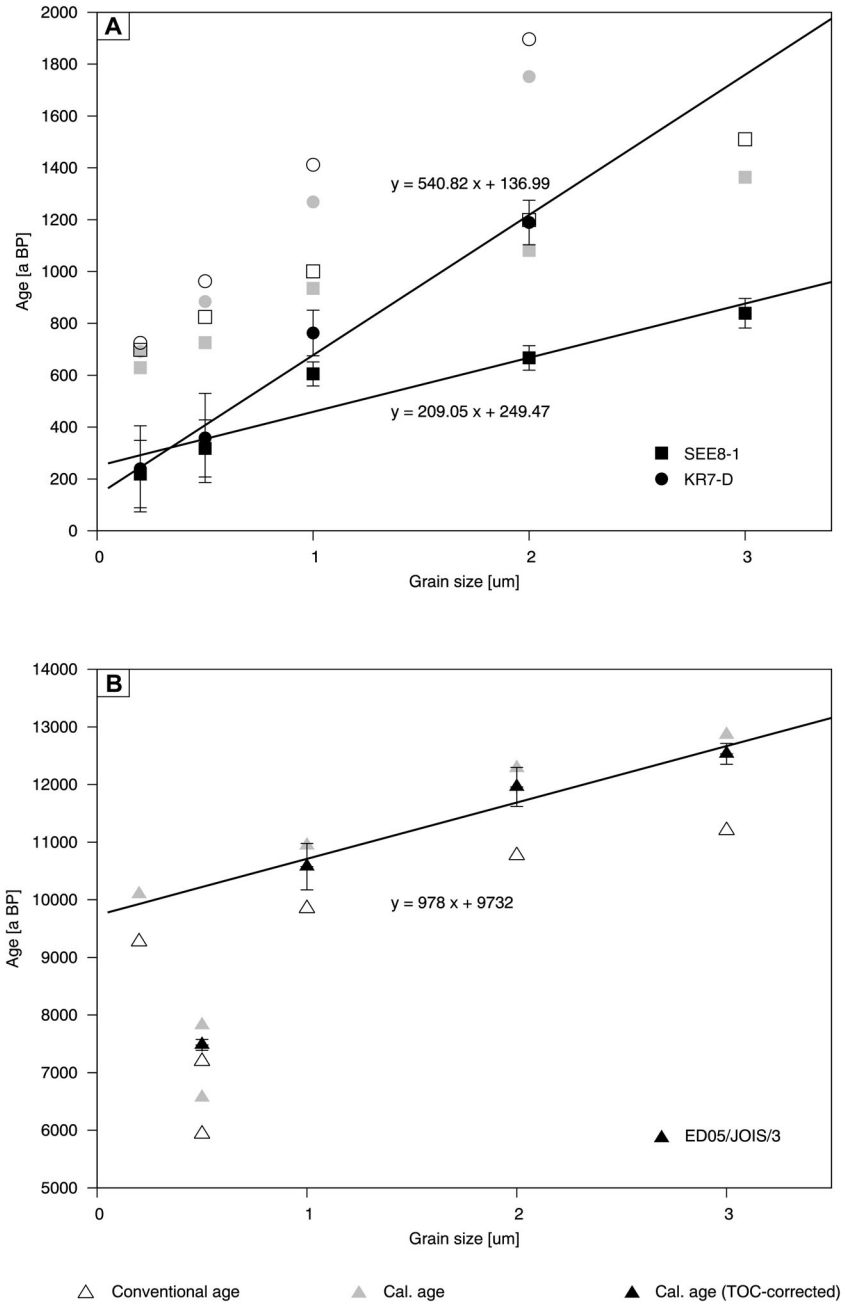

Fig. 8. Calculated radiocarbon ages from different grain-size fractions: (i) radiocarbon ages calculated from measured $F^{14}C$ values (conventional ages; empty symbols); (ii) calibrated ages from measured $F^{14}C$ data (grey symbols); and (iii) calibrated ages from total organic carbon (TOC)-corrected $F^{14}C$ values (filled symbols). (A) Modern lake sites; and (B) ancient lake sediment from Site ED05/JOIS.

However, because the ^{14}C activity decreases over the last 25 kyr (Reimer *et al.*, 2020), the calibration would roughly account for the combined effect of the different sources.

Results of this calculation show that the maximum age of organic matter, being degraded at the time of carbonate precipitation, would be around 2000 years (see Table S1 for details). Assuming this age for TOC yields radiocarbon ages that are on the order of 500 years younger, and this shift is similar for old and young ages (Table 1, column 'Age corr.'; Fig. 8). The effect does not change the overall magnitudes and trends, nor rates, but it shows that the finest

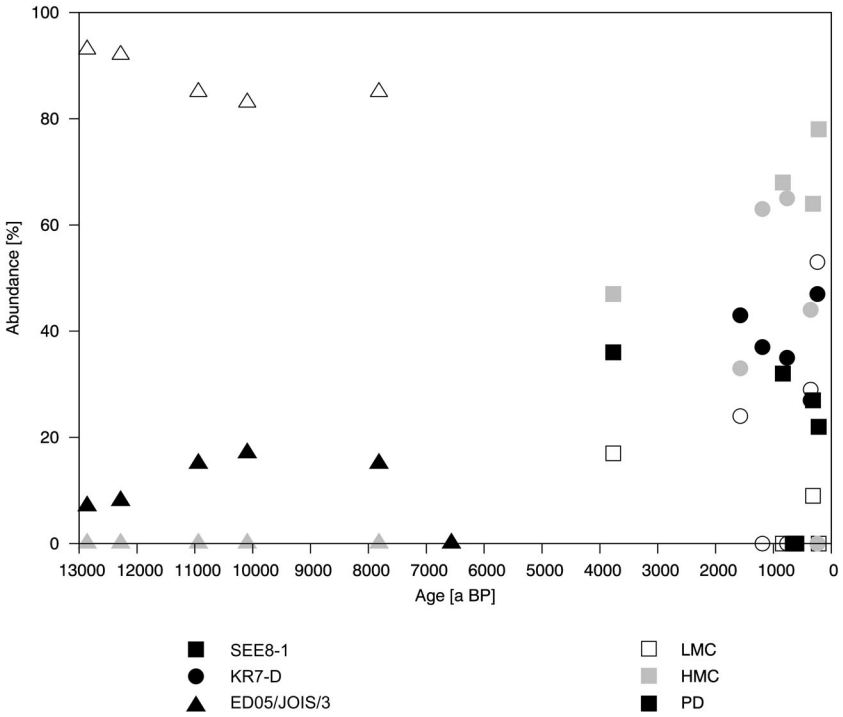

Fig. 9. Radiocarbon ages [calibrated and total organic carbon corrected] in comparison with relative abundance of the carbonate phases low-Mg calcite (LMC), high-Mg calcite (HMC) and protodolomite (PD) at the three locations SEE8, KR7 and ED05/JOIS. At the modern lake sites, protodolomite increases with age, suggesting slow formation, possibly due to ripening. In contrast, HMC is most abundant in the younger size fractions and remains present also in older fractions. Low-Mg calcite does not show a significant trend with age. In contrast, sample ED05/JOIS/3 shows a high abundance of LMC and low PD, but no HMC.

fractions (<0.2 μm) reach a modern age, within the error of the dating method (due to the input of anthropogenic CO_2 into the atmosphere, samples formed after *ca* 1850 AD yield approximately the same radiocarbon age, which leads to a large uncertainty). Hence, it is reasonable to assume that carbonates in Lake Neusiedl are still forming today, at least episodically, if the conditions are favourable.

Authigenic versus detrital carbonates

A further effect that could influence radiocarbon ages is the presence of detrital carbonate lacking ^{14}C. Although carbonates are primarily affected by chemical weathering, physical erosion supplies fine grain sizes that can be transported by water and wind. Sharp peaks in XRD patterns could indicate detrital calcite and dolomite particles, because Triassic to Neogene sediments from the source area comprise predominantly well-defined stoichiometric compositions of LMC and dolomite. X-ray diffraction patterns of the >3 μm fraction record distinct peaks for a calcite with low $MgCO_3$ content (≤2 mol%) and (proto)dolomite with 49 to 51 mol% $MgCO_3$ (Figs 3 and 4; Table 2), whereas diffractograms of smaller grain-size fractions exhibit up to three broad diffraction peaks indicating carbonate phases of variable Mg content (Fig. 3B; Table 2). The latter carbonate phases are most certainly authigenic as they would be metastable over geological timescales; but also, the phase with dolomitic stoichiometry is largely metastable protodolomite, since the 015 ordering peak is either extremely small or absent. This indicates that carbonate phases are predominantly authigenic in origin.

An authigenic origin of most carbonate phases in the Lake Neusiedl sediments is further supported by SEM observations, showing rhombohedral, and somewhat irregular, crystals consisting of nanocrystalline rhombs arranged with coherent orientation (Fig. 5; Meister *et al.*, 2023). SEM did not show angular or subangular carbonate particles that could be clearly assigned to a detrital origin.

A contribution of detrital carbonate leads to older ages in the larger grain-size fractions, while

the small grain sizes approach modern ages. In particular, sample SEE8-1 shows an age of 3644 cal yr BP in the >3 μm fraction. This age is considerably older compared to the smaller size fractions of this sample, even if the trend line would be extrapolated to include the fraction in which all grain sizes >3 μm are integrated (Fig. 7). While a contribution of detrital carbonate grains eroded from carbonate bedrock is regarded as minor, for the reasons explained above, older authigenic carbonate could be derived from pre-Holocene lake deposits exposed on land, as, for example, at location ED05/JOIS. In any case, data of the coarse fractions should be interpreted with caution.

Sample homogeneity

Due to homogenization of the sediment, the measured radiocarbon activity represents average values, i.e. individual carbonate crystals may be older or younger than the bulk average. Although the samples were well-homogenized and replicates of stable isotope and radiocarbon measurements agree within the uncertainty of the measurement, a considerable scatter in $\delta^{13}C$ among the grain-size fractions of sample ED05/JOIS/3 (0.5 to 1.0 μm and 2 to 3 μm) most likely indicates heterogeneity for those samples.

The three identified carbonate phases (LMC, HMC and PD) cannot be mechanically or chemically separated; therefore, stable isotope and radiocarbon data of Lake Neusiedl samples have to be interpreted carefully. Different grain-size fractions from each sampling site consist of the three carbonate phases in different proportions (Fig. 4), but no trends between mineral abundances and isotope values are apparent. Despite mixing, the age trends with grain size are systematic and suggest that the average age shifts with grain size. Using calibrated average ages represents a meaningful estimate, as the calibration curve shows a more or less continuous decrease in the abundance of ^{14}C over time.

As is known from sequential leaching of fine-grained dolomite from Deep Springs Lake (Peterson *et al.*, 1963), crystals may grow stepwise, with concentric zones showing outward decreasing ages (see Meister *et al.*, 2023). Hence it has to be considered that the cores of some grains are older than the age derived from the average radiocarbon activity, while the rim may be younger or even modern. This needs to be taken into account for the subsequent discussion of growth rates.

Overprint due to recrystallization

As shown by multiple studies, authigenic carbonates may undergo transformation from HMC to PD and LMC (e.g. Hardie, 1987; Budd, 1997; Rodriguez-Blanco *et al.*, 2015; Kell-Duivestein *et al.*, 2019; Fussmann *et al.*, 2020; Pina *et al.*, 2022). Therefore, percentages of carbonate phases from our samples were compared with measured radiocarbon ages (Fig. 9). While the data are quite varied, it is noticeable that the proportion of Mg-calcite is particularly high in the younger size fractions. At the same time, the proportion of PD is low in the youngest samples of modern lake sediments. This would support the scenario proposed by Fussmann *et al.* (2020) and Meister *et al.* (2023) that HMC initially precipitates and is subsequently transformed into PD. Alternating episodes of concentric growth and ripening would occur under variable conditions while the grains are suspended in the water column or the benthic boundary layer.

Transformation processes could reset the ^{14}C age. Therefore, measured ages may represent minimum ages. However, considering that the measured ^{14}C ages are rather old, it is reasonable to assume that ^{14}C signatures were probably conserved during ripening. As observed by Fussmann *et al.* (2020), metastable phases do not show much change downcore, which suggests that these phases remain preserved in the presence of sedimentary porewater. Once buried, the mineral assemblage preserves most of its ^{14}C content. The exact mechanism will be discussed below, in the section *Ripening of metastable carbonate phases*.

In contrast to modern lake sediments, the older lake sediment from site ED05/JOIS does not contain HMC. Most likely, former HMC was replaced by PD over time. Also, LMC is predominant in the sediment of site ED05/JOIS compared to modern lake sediments, which may be due to a different lake chemistry, for example, different Mg/Ca ratio of the lake water, in the past.

Rates of precipitation

Radiocarbon activity decreases with increasing grain size and thus records growth of authigenic minerals over time. The correlation between grain size and radiocarbon age is linear, if some outliers such as the fraction >3 μm are excluded. The relation between grain size and age is, however, not straightforward. It can be

assumed that a crystal is oldest at its core and concentric growth zones are progressively younger moving from the centre to the edge. The measured radiocarbon age represents the average age of the grain. As an approximation, the rhombohedral carbonate crystals were treated as cubes. With every time step, the age of the entire grain increases in proportion to the volume of the newly accreted layer. At a small step size, the resulting age to grain-size function is nearly linear and can be fitted with a regression line (Fig. 8). To fit the regression lines, it was assumed that also the most recent growth layer has a minimum age, which is 270 cal yr BP for Site SEE8 and 180 cal yr BP for Site KR7. These ages are, however, within the resolution of the radiocarbon data, i.e. they are regarded as modern.

This calculation resulted in a normal growth rate (i.e. growth perpendicular to the crystal surface) of 0.60 μm/ka at the open lake site (SEE8), and 0.23 μm/ka at site KR7. The reason for the difference between the two sites is not entirely clear. Because Lake Neusiedl has experienced variable environmental conditions ranging from high lake levels to dry episodes during the past centuries (Sauerzopf, 1959; Draganits *et al.*, 2022) crystal growth was most likely discontinuous and possibly episodic. Hence, the obtained growth rates represent long-term (centennial-scale) average values. Moreover, sediment dynamics varies between different sites, as indicated by the variable sediment thickness (Heine *et al.*, 2016). Presumably, re-suspension varies from site to site, and also the reeds attenuate waves and currents and may therefore trap sediment. Presumably, crystal growth stops when the carbonate grains are buried and chemically equilibrated with the pore water (as further discussed below).

The obtained normal growth rate corresponds roughly to half of the growth rate of the rhombohedral edge length. In comparison, rhombohedral growth rates determined by ^{14}C dating of sequentially leached grains in Deep Springs Lake record a maximum rate of about 0.5 μm/ka (Peterson *et al.*, 1963, fig. 7). These values are in good agreement with those of site KR7 in Lake Neusiedl, whereas the growth rate at site SEE8 is about twice as high.

In contrast to modern lake sediments, growth rates determined for grain-size fractions of old lake sediments from ED05/JOIS are considerably lower (around 0.13 μm/ka; Fig. 8B). It is possible that the chemical composition of the lake water or the hydrology (with episodic dry periods) at that time was different, resulting in lower average precipitation rates. Like Lake Neusiedl today, the older lake was affected by re-suspension due to wind and waves. It is likely that old sediments were mixed several times resulting in a re-distribution of carbonates of different age which ultimately results in more homogeneous ages of different grain sizes, and would be expressed in lower apparent growth rates. In contrast, in the modern open lake, the sediment layer is thinner and mixing would have involved a smaller age range.

Timing of nucleation

Using the herein calculated growth rate, the time of nucleation for a cubic crystal (as an approximation of a rhombohedral calcite crystal) can be estimated. The resulting ages reveal that the nuclei are surprisingly old. For 3 μm sized grains a nucleation age of *ca* 2700 cal yr BP (as estimates are based on calibrated ages) was obtained for the open lake site SEE8, and *ca* 6600 cal yr BP for site KR7 in the reed belt. Larger grains would suggest even higher ages.

For the old lake deposits from site ED05/JOIS, the nuclei of 3 μm grains yielded ages of *ca* 25 cal ka BP, i.e. the range of nucleus ages in larger grain-size fractions would include the entire last glacial maximum (*ca* 26 to 20 ka BP; Ivy-Ochs *et al.*, 2022). This potentially high age has to be taken into account for reconstruction of the environmental evolution of Lake Neusiedl as well as the nucleation and growth mechanism of authigenic Ca-Mg-carbonates.

Implications for sedimentation rates

Given the normal growth rate of carbonate mineral surfaces, this value can be extrapolated to estimate the volume gain for the whole sediment in order to obtain average sedimentation rates, using the porosity, carbonate content (from STA) and grain-size distribution (from the Sedigraph curve for sample KR7-D; Fig. S3). The grain-size distribution can be approximated by a lognormal distribution (Middelburg *et al.*, 1997), which yields an average grain volume and average volume change per time, for the entire population of grains. Based on this information and using a growth rate of 0.6 μm/ka, a sedimentary layer doubles about every 3500 years, assuming constant growth. This number decreases if precipitation occurs episodically. More critically, the sedimentation rate also depends on how much sediment is suspended in the water

column and how much of the sediment column was repeatedly re-suspended. High pH causes the water to be turbid, keeping particles flocculated and in suspension. Although the pH measurements over the last 20 years appear very stable (Fig. S1), influx of lower pH water would result in sinking of the particles while precipitation would be discontinued.

The considerably lower crystal growth rate of 0.13 μm/ka at site ED05/JOIS results in sedimentation rates in the order of 16 000 years to double the homogenized sediment layer. This low apparent sedimentation rate is calculated from older ^{14}C ages and suggests that authigenic carbonate precipitation had already started during the Late Glacial. The oldest radiocarbon age was determined in sample ED05/JOIS/3 which yielded a calibrated age of 15 cal ka BP in the >3 μm size fraction. In comparison, a fragment of a bivalve shell from the same pit (sample ED05/JOIS/2, 2.6 m depth, i.e. 115.0 m a.s.l.; Draganits *et al.*, 2022) yielded an age of 14.4 cal ka BP and is thus in excellent agreement with the proposed age of the authigenic carbonate fraction. Moreover, the very old back-calculated nucleation age of around 25 cal ka BP suggests the onset of lake sedimentation before or during the last glacial maximum.

The obtained sedimentation rates are orders of magnitude lower than those of authigenic calcite deposition in temperate freshwater lakes (e.g. Hsü & McKenzie, 1985; Teranes *et al.*, 1999). Explanations for this large difference may be: (i) Sediment in suspension could have been lost to the Danube, during periods of flooding. Drainage could have been episodically high before construction of the dams (Draganits *et al.*, 2022). Also, at times of desiccation, aeolian deflation could have removed significant amounts of sediment. However, this explanation is not supported by the extremely slow growth rate of the carbonate crystals. Also, such an effect would probably have removed a great part of the fine fraction. (ii) Significant amounts of carbonate may dissolve. Although dissolution–reprecipitation may indeed occur, resulting in the transition of Mg-calcite to PD (Fussmann *et al.*, 2020; Meister *et al.*, 2023) and LMC, the grains do not show clear signs of dissolution. (iii) Precipitation was very slow, reflecting the rather slow contribution of ions from inflowing water, and perhaps also the episodic removal of ions by outflowing solutions. Despite episodes of strong evaporation in the past, evaporative concentration has led to only slow authigenic carbonate precipitation of both carbonates and silicates. Diatoms produce amorphous silica frustules, which are rapidly dissolved due to the elevated pH. In turn, silica is mostly incorporated into authigenic clay minerals, as shown in experiments by Molnár *et al.* (2021). At the same time, the supply of detrital sediment is very low (due to the flat topography). All in all, this lake is characterized by very low sedimentation rates that may have prevailed for thousands of years.

Environmental conditions during mineral formation

Environmental conditions are well-reflected by the oxygen isotope composition of the carbonates. All samples except subsample KR7-D 0.2 to 0.5 μm have $\delta^{18}O$ values between −3.6‰ and −0.4‰ VPDB. This range and the annual temperature range of 0 to 30°C were used to calculate the oxygen isotope composition of lake water at the time of carbonate precipitation. Using the fractionation factor of Kim & O'Neil (1997; assuming that all carbonate is calcite) results in $\delta^{18}O$ values for the water of −0.2 to 3.0‰ (Vienna Standard Mean Ocean Water; VSMOW) at 30°C and −6.6 to −3.4‰ VSMOW at 0.1°C for the water under the assumption of isotopic equilibrium. This falls into the range of measured $\delta^{18}O$ values of Lake Neusiedl water between −6‰ and −1‰ VSMOW (Baranyi *et al.*, 1994; Rank *et al.*, 2016; Schnedlitz, 2020) with a noticeable seasonality between winter (low values) and summer (high values). These values indicate the influence of meteoric water during the winter months and of evaporation during the summer months. The relatively high values are atypical for freshwater lakes (e.g. McKenzie & Hollander, 1993; Teranes *et al.*, 1999; Teranes & Bernasconi, 2005) as they reflect the shallow water depth and high evaporation of Lake Neusiedl (cf. Reitinger *et al.*, 1991; Boroviczény *et al.*, 1992; Sailer & Maracek, 2019). The most extreme value of 9.2‰ measured in sample KR7-D (only in the 0.2 to 0.5 μm size fraction but verified by replicate measurements) suggests formation during an episode of extreme evaporation. It cannot be resolved whether and how the isotope values vary between different mineral phases, presumably formed during different seasons. Moreover, the oxygen isotope composition is likely reset during recrystallization, so that partial equilibration may also occur during winter. This could explain the slight decrease in $\delta^{18}O$ with grain size (and age), while the smallest grain sizes

(<0.5 μm) may be subject to more dynamic conditions.

Oxygen and carbon isotope values correlate in modern Lake Neusiedl sediments, which is commonly observed in evaporative lakes (e.g. Talbot, 1990; Hofbauer *et al.*, 2021), even though C and O isotopes are not per se coupled. This trend may reflect meteoric water input that is coupled to a higher supply of ^{13}C-depleted DIC from degrading organic matter (for example, from soil).

Seasonal variations of ionic compositions of lake water over time (Fig. S1) show an increasing trend during the summer months, which is related to seasonal evaporative concentration. However, long-term trends of the last 20 years show higher amplitudes than seasonal variations, where the total ions more than double (Fig. S1). As the total ionic content changes, so does alkalinity due to the conservative ion balance (Fig. S2). This change in alkalinity is balanced by equilibration with atmospheric CO_2, so that the pH remains rather constant. With increasing alkalinity and ionic concentrations, the saturation states of calcite and dolomite also increase (Fig. S2).

Calcium concentration in the lake water shows the opposite trend, i.e. higher concentrations in winter and lower ones in summer (Fig. S1), suggesting precipitation of Ca-Mg-carbonate at times of high supersaturation (Blohm, 1974; Wolfram *et al.*, 2021; Figs S1 and S2). While the Ca^{2+} concentration may drop by half a mmol/l due to precipitation, Mg^{2+} may further increase due to evaporative concentration. As Mg-levels are almost ten-fold higher, the effect of precipitation is not so visible for Mg. Assuming that the precipitate consists of Mg-calcite with a stoichiometric composition of 30% $MgCO_3$, a carbonate content of 60% of the sediment and a porosity of 0.7, a sedimentation rate on the order of 10 cm/ka can be estimated. This would be in line with the sedimentation rate based on ^{14}C given above. This would also be sufficient to create the sediment cover that was deposited over several thousand years.

Remarkable for the lake water chemistry is an excess of Mg over Ca, which is in contrast to the Wulka River, the main tributary, with an average Mg/Ca ratio around 0.7 (Berger & Neuhuber, 1979; Schnedlitz, 2020). How much groundwater recharge contributes to the ion balance is not clearly known (see Tchaikovsky *et al.*, 2019). This Mg/Ca ratio is in the range of the total sediment composed of a mixture of LMC, HMC and PD. An excess of Mg in the solution could be caused by different kinetics of the carbonate minerals. If this was the case, a small excess of Mg could then be amplified by HMC precipitation, as the Mg/Ca ratio in the precipitate does not exceed a 1 : 1 ratio. The additional Na-related alkalinity helps to draw down Ca^{2+} to very low concentrations (see Wolfram *et al.*, 2021).

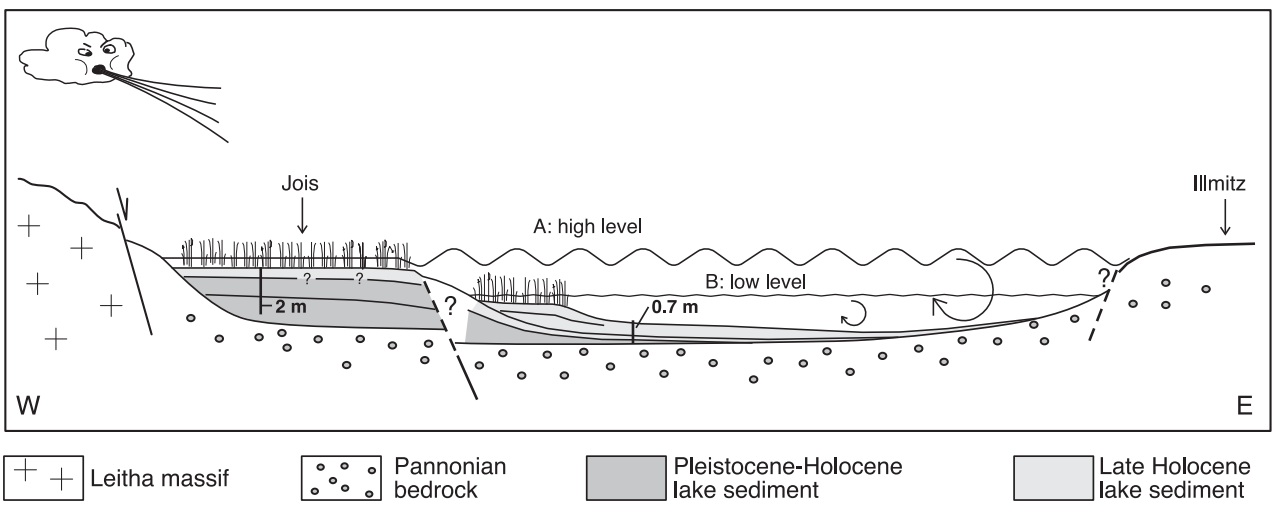

Fig. 10. Schematic representation of lake evolution over time. (A) Scenario of a deeper lake at times of a cooler and more humid climate (highstand), and strong internal sediment redistribution. An extended reed belt may have further contributed to sediment trapping. (B) Scenario of the present state of the lake, with higher evaporation and lower lake level. Besides palaeoclimate changes, also tectonic faulting may have created accommodation space for the modern lake basin.

Besides evaporative concentration and carbonate precipitation, Mg-content, and to a minor extent also Ca, may be further influenced by adsorption and incorporation into the interlayers of clay minerals, in particular of smectite, which has been detected by XRD in this study's samples (Fig. 3). Adsorption and desorption equilibria are largely controlled by pH, temperature and salinity (Krachler *et al.*, 2000). Moreover, smectites may form at high concentrations of Mg and silica, and high pH (Bristow *et al.*, 2012).

Environmental evolution of the lake during the Holocene

No significant relationship between the C-isotope and O-isotope composition and the radiocarbon age was observed in modern Lake Neusiedl sediments, that would provide a hint for a temporal evolution of the lake environment. Also, the increase of PD with age may indicate ripening rather than a changing lake environment.

Significant changes are caused by anthropogenic activity: melioration measures including the diversion of the Rabnitz River, documented in a report from 1568 (Draganits & Gmasz, 2023), the completion of a dam road in 1780 that successively separated the present-day lake from its water supply from the south and east, and the excavation of a canal completed 1909/1910 (Draganits *et al.*, 2022). Therefore, the modern hydrological setting is vastly different from the pre-16th century situation. The changes caused by melioration after 1568 can, however, not be resolved by ^{14}C dating. Lake level fluctuations were probably more pronounced before this period, with high levels due to river input, interrupted by low levels due to desiccation or outflow into the Danube. The lake was virtually dry between 1865 and 1870 and very low in the winters of 1917/1918, 1924/1925 and 1933/1934 (Draganits *et al.*, 2022). Such periods of dryness must have caused breaks in carbonate precipitation and deposition. Also the influx of low pH water from tributaries resulting in a decrease in carbonate saturation could have caused periodical cessation of carbonate precipitation.

The ^{14}C ages of the Mg-rich carbonate mineral assemblage suggest that the dynamic chemistry of the lake persisted for a long time, going back to at least 3700 cal yr BP (oldest calibrated ^{14}C age) and perhaps even to more than 8000 cal yr BP (inferred oldest nucleation age based on calibrated ages). Lake Neusiedl can therefore be regarded as a Holocene phenomenon. Most likely, due to the extremely flat topography, any preceding Pleistocene lake deposits either did not form within the present lake area, or they were removed by erosion, so that the Holocene deposits within the present lake rest on Pannonian clayey bedrock.

Implications for the early evolution of the lake system

Sample ED05/JOIS/3, taken outside the modern lake, contains on average more than 80% LMC, subordinate PD and no HMC. δ^{18}O values of this sample range between −0.8‰ and −2.9‰ and are in the same range as those from the other two localities. In contrast, the δ^{13}C values of sample ED05/JOIS/3 (−1.69 to −0.39‰) are 1.5 to 3.0‰ higher compared to samples SEE8-1 and KR7-D. The presence of LMC accompanied by higher δ^{13}C values suggests conditions more similar to a freshwater lake. The Mg/Ca ratio at that time was probably lower, and the DIC pool less influenced by organic matter. The lake was probably deeper and affected by more freshwater input, presumably during a cooler and locally more humid climate. Even a somewhat deeper lake (cf. today's Balaton Lake; e.g. Müller, 1970; Nyirö-Kósa *et al.*, 2018; Molnár *et al.*, 2021) could still have been dominated by evaporation, as reflected by the oxygen isotope composition, which differs from a freshwater lake.

Radiocarbon data from site ED05/JOIS yield a calibrated age of 15.5 cal ka BP and a potential onset of nucleation around 25 ka BP. This corresponds to the period within the last glacial maximum (see summary of records in the Eastern Alps by Heiri *et al.*, 2014). The study area was never glaciated and only affected by periglacial permafrost. Clearly, the sedimentary section at site ED05/JOIS is thicker (>2 m) than the Holocene lake infill and cannot be found in today's Lake Neusiedl below the Holocene layer that directly overlies Pannonian clay. The top of the section at site ED05/JOIS is >2 m higher than today's water table. This may indicate a deeper lake basin, where sediment distribution was highly uneven (see scenario in Fig. 10). Such a variable sediment distribution could be explained by stronger winds, but also by sediment trapped in a reed belt. Both effects are also observed today, even though at a smaller magnitude. Another explanation could be differential subsidence of the lake basin due to tectonic faulting or differential compaction of the underlying Neogene sediment. Indeed, faults running parallel to the margin of the Leitha range have

been observed in seismic profiles (Loisl *et al.*, 2017; Zámolyi *et al.*, 2017) and they are indicated by dashed lines in Fig. 10.

Implications for pathways of authigenic carbonate formation

Radioisotope ages and the calculated growth rates provide unprecedented insight into the precipitation of Ca-Mg-carbonates and ripening of HMC to PD and eventually ordered dolomite. In Lake Neusiedl, these processes appear to be still ongoing which offers an opportunity to assess the controlling thermodynamic and kinetic factors in the surrounding environment.

Supersaturation

At least three distinct carbonate phases with different Mg content are present in Lake Neusiedl. This may indicate that different types of nuclei form(ed) under different initial conditions or, as suggested by Meister *et al.* (2023), re-ordering occurs via recrystallization under variable conditions. Saturation indices calculated from lake water chemistry (Fig. S2) are around one for calcite and three for dolomite. This is consistent with calculations by Fussmann *et al.* (2020) and Schnedlitz (2020), which show that all carbonate phases are supersaturated in the lake water. Seasonal and multi-annual increase in ion concentrations and alkalinity may cause a variation of the SI by up to one unit, so that an increase in supersaturation could induce nucleation of carbonate phases.

On the other hand, the more soluble carbonate phases, such as HMC, may become undersaturated, either due to ion depletion in the winter months (cf. Figs S1 and S2) or due to a drop in pH (e.g. Blohm, 1974; Wolfram *et al.*, 2021). While the pH is relatively stable in the water column (between 8.5 and 9.5; Schnedlitz, 2020), Fussmann *et al.* (2020) recorded a drop in pH near the benthic boundary layer, where mixing with porefluid and, presumably, organic acids could further lower the pH. Under these conditions it is possible that HMC becomes locally and temporally undersaturated. These authors then proposed that undersaturation may cause recrystallization. A similar scenario of dolomite growth was proposed for other evaporative lakes, such as Deep Springs Lake (Meister *et al.*, 2011a,b) and Lake Van (McCormack *et al.*, 2018). Despite the high alkalinity in these environments, carbonate supersaturation is limited due to the relatively low concentrations of cations. Due to the dynamic conditions in the water column and in the benthic mixing layer, waters may be temporally undersaturated with respect to the more soluble carbonates.

Fussmann *et al.* (2020) showed that the pore water of the sediment remains saturated with regard to carbonate phases. This would prevent the dissolution of HMC and therefore prevent recrystallization to PD in the buried sediment.

Kinetic barrier

While a range of carbonate minerals are oversaturated in the lake water, reaction kinetics determines which mineral phase forms first. Under ambient conditions in Lake Neusiedl, most likely HMC with a range of stoichiometric compositions (10 to 20 mol% Mg) forms first, even though representing a metastable phase (e.g. Sandberg, 1983; Johnson & Goldstein, 1993). This is not unusual, as often the most soluble phases form first, because they tend to have a lower energy barrier due to their lower interfacial energy – this is commonly referred to as Ostwald's step rule (Ostwald, 1897). In this way, at high supersaturation, amorphous calcium carbonate (ACC) or amorphous calcium–magnesium carbonate was observed as precursor phase in laboratory studies (e.g. Rodriguez-Blanco *et al.*, 2012; Zhang *et al.*, 2012; Purgstaller *et al.*, 2016; Blue *et al.*, 2017) but, so far, not in Lake Neusiedl.

As shown in the experiments by Rodriguez-Blanco *et al.* (2015), PD forms more sluggishly. Dolomite, often the most supersaturated phase in marine and lacustrine environments, is inhibited by a high kinetic barrier (Land, 1998). Precipitation studies under controlled laboratory conditions show that dolomite crystallization on a well-ordered dolomite surface in supersaturated solution will stop after two monolayers (Higgins & Hu, 2005; Fenter *et al.*, 2007). Dolomite formation may proceed extremely slowly, which is also supported by the high ^{14}C ages in this study. For this reason, dolomite is widely considered not as a primary phase nucleating directly from the water column, but as a diagenetic (Machel, 2004) or 'penecontemporaneous' product (Budd, 1997). It is widely accepted that dolomite may form via ripening of a metastable precursor (Nordeng & Sibley, 1994; Sibley *et al.*, 1994; Deelman, 1999). The reason is that, according to Ostwald's step rule, the metastable phase forms first.

The nature of the kinetic barrier for dolomite formation is still incompletely understood.

Lippmann (1973) proposed the concept that water molecules strongly bind to Mg-ions and that dehydration imposes a strong energy barrier, and recent studies proposed that diverse factors, such as organic matter, microbes or clay minerals, may have an effect on the dehydration of Mg (see discussion in Fussmann *et al.*, 2020; and references therein). However, this does not explain why the kinetic barrier affects, specifically, dolomite, while Mg-calcite readily forms. Instead, it is possible that kinetic barriers specifically affect the mineral surface, but the exact nature of this presumed energy barrier is not known.

Ripening of metastable carbonate phases

Slow transformation of HMC to PD and LMC could have occurred in samples from this study. Indeed, grain-size fractions in modern lake sediments containing more PD show a higher ^{14}C age, which suggests that PD forms at a lower rate as a result of ripening, while fractions showing a young age contain abundant HMC (Fig. 9). These findings might indicate that the precursor HMC undergoes transformation to PD, and some HMC may also transform to LMC. In addition to the major phases detected by XRD, which are essentially part of a compositional continuum, Meister *et al.* (2023) observed micrometre-scale rhombohedral crystals showing Mg-poor and Mg-rich zones. The Mg-poor zones show signs of dissolution, suggesting a replacement of HMC by PD. Moreover, high-resolution transmission electron microscope images revealed nano-scale dolomitic domains within PD, in coherent orientation with the host crystal lattice. Meister *et al.* (2023) proposed a scenario where nanodomains form as nanocrystals at the recrystallization front and then become incorporated in an oriented way in the crystal lattice of the PD.

High Mg-calcite readily nucleates and grows in the water column, and also ripening may occur while the growing crystals are held in suspension. During this process, then, re-suspension and ripening in the water column would not be a diagenetic process. This view is supported by the observation that the metastable phases HMC and PD remain in the deeper buried layers (at 30 cm depth or deeper; Fussmann *et al.*, 2020). The reason for this longer-term preservation of metastable phases could be that the pore water remains saturated with respect to the metastable phase (HMC). Ripening to PD (and dolomite nanodomains) may occur under fluctuating conditions in the water column or the benthic mixed layer, while the metastable minerals are stabilized within the buried sediment. This mechanism may explain the long-term stability of metastable authigenic phases in Lake Neusiedl sediment, while ripening only occurs during short episodes of re-suspension and mixing.

In contrast to the modern lake sediments, HMC has not been detected in the older lake sediments at site ED05/JOIS. This is to be expected, since these sediments are older than 6000 cal yr BP and decoupled from the modern lake water where precipitation of HMC is ongoing. The PD content is also much lower than in modern lake sediments, and the predominant phase is LMC, indicating different water chemistry, possibly due to different climatic and/or hydrological conditions.

CONCLUSIONS

Calcium–magnesium carbonate phases in modern, unconsolidated sediments of Lake Neusiedl consist of a continuum of Mg-calcite phases with the predominance of high-Mg calcite (HMC) with 10 to 20 mol% $MgCO_3$ and protodolomite (PD) with 40 to 50 mol% $MgCO_3$, as well as traces of low-Mg calcite (LMC). Moreover, older lake deposits show predominantly LMC with minor amounts of PD. Based on the poorly defined stoichiometry and an 015 ordering of dolomite near the detection limit, the identified carbonate phases are predominantly authigenic in origin. Radiocarbon ages of these authigenic carbonates from the lake increase with grain size from 200 cal yr BP in the <0.2 μm fraction to 3700 cal yr BP in the >3 μm fraction. The youngest sample yielded a modern age, so that it is possible that suspended carbonate crystals are still growing today in the lake water column. The obtained growth rate of grain surfaces between 0.23 μm/ka and 0.60 μm/ka is extremely slow, but within the range of dolomite growth rates observed in other evaporative lakes. The PD content only increases in older grain-size fractions, while HMC is present in the youngest fractions, suggesting that PD forms by ripening of HMC. An estimated nucleation age between 3600 and 8000 cal yr BP suggests that the present Lake Neusiedl persisted during most of the Holocene and experienced extremely low sedimentation rates. Authigenic mineral formation was mainly driven by variable humid and evaporative conditions at high pH and elevated salinity. Fluctuating environmental conditions may be responsible

for the ripening of HMC to PD, and incipient dolomite formation.

In contrast to the modern lake, older lake sediments with radiocarbon ages between 6 and 15 cal ka BP, suggest a growth rate of 0.13 μm/ka. The extrapolated nucleation age goes back to more than 25 cal ka BP, suggesting the presence of a lake during the last glacial maximum. This precursor lake was at least episodically deeper, and its water contained less Mg, but its chemistry was already dominated by evaporation.

ACKNOWLEDGEMENTS

Field and laboratory support, as well as assistance with data access and artwork were provided by Gerald Auer, Ina Böhm, Sandra Braumann, Richard Haiderer, Alois Herzig, Franko Humer, Ilse Koglbauer, Michael Ladich, Klaus Mair, Friederike Neuhuber, Daniela Schaferl and Monika Wimmer. Bo Liu provided input for the calculation of sedimentation rates. SN was funded by project H2471/2012 of Hochschuljubiläumsstiftung der Stadt Wien and by the Back to Research Grant of the University of Vienna. ED was funded by project H-990-2004 of the Hochschuljubiläumsstiftung der Stadt Wien. Ola Kwiecien, Andrea Martín Pérez, and an anonymous reviewer are acknowledged for their comments and suggestions on earlier versions of this manuscript.

DATA AVAILABILITY STATEMENT

All data are included in the manuscript.

REFERENCES

Arnold, J.R. and **Libby, W.F.** (1949) Age determinations by radiocarbon content: checks with samples of known age. *Science*, **110**, 678–680.

Auer, B. and **Dick, G.** (1994) Der See und die Lacken - ein limnologischer Überblick. In: *Vogelparadies ohne Zukunft? Ramsar-Gebiet Neusiedler See – Seewinkel* (Eds Dick, G., Dvorak, M., Grüll, A., Kohler, B. and Rauer, G.), pp. 45–60. Umweltbundesamt, Wien.

Bácsatyai, L., **Csaplovics, E.**, **Márkus, I.** and **Sindhuber, A.** (1997) Digitale Geländemodelle des Neusiedler See-Beckens. *Wissenschaftliche Arbeiten aus dem Burgenland*, **97**, 1–53.

Balci, N., **Menekşe, M.**, **Karagüler, N.G.**, **Sönmez, M.S.** and **Meister, P.** (2016) Reproducing authigenic carbonate precipitation in the hypersaline Lake Acıgöl (Turkey) with microbial cultures. *Geomicrobiol. J.*, **33**, 758–773.

Baranyi, S., **Deál, J.**, **Dreher, J.**, **Mahler, H.**, **Major, P.**, **Neppel, F.**, **Papesch, W.**, **Rajner, V.**, **Rank, D.**, **Reitinger, J.** and **Schmalfuss, R.** (1994) Wasserhaushaltsstudie für den Neusiedlersee mit Hilfe von Geochemie und Geophysik. In: *Jubiläumsschrift 20 Jahre Geologische Zusammenarbeit Österreich – Ungarn. Teil 2* (Eds Lobitzer, H., Császár, G. and Daurer, A.), pp. 419–435. Geologische Bundesanstalt, Wien.

Berger, F. and **Neuhuber, F.** (1979) The hydrochemical problem. Neusiedlersee: Limnology of a Shallow Lake in Central Europe. *Monograph. Biol.*, **37**, 89–99.

Bischoff, W.D., **Bertram, M.A.**, **Mackenzie, F.T.** and **Bishop, F.C.** (1993) Diagenetic stabilization pathways of magnesian calcites. *Carbonates Evaporites*, **8**, 82–89.

Blohm, R. (1974) *Sedimentpetrographische Untersuchungen am Neusiedler See/Österreich*. Unpublished PhD thesis. University of Heidelberg, Heidelberg.

Blue, C.R., **Giuffre, A.**, **Mergelsberg, S.**, **Han, N.**, **De Yoreo, Y.Y.** and **Dove, P.M.** (2017) Chemical and physical controls on the transformation of amorphous calcium carbonate into crystalline $CaCO_3$ polymorphs. *Geochim. Cosmochim. Acta*, **196**, 179–196.

Bontognali, T.R.R., **Vasconcelos, C.**, **Warthmann, R.J.**, **Bernasconi, S.M.**, **Dupraz, C.**, **Strohmenger, C.J.** and **McKenzie, J.A.** (2010) Dolomite formation within microbial mats in the coastal sabkha of Abu Dhabi (United Arab Emirates). *Sedimentology*, **57**, 824–844.

Boroviczény, F., **Liebe, P.**, **Neppel, J.**, **Pinczes, J.**, **Rank, D.**, **Schmalfuß, R.**, **Deak, J.**, **Mahler, H.**, **Papesch, W.**, **Pajner, V.**, **Reitinger, J.** and **Takats, T.** (1992) *Wasserhaushaltsstudie für den Neusiedlersee mit Hilfe der Geophysik und Geochemie 1980–1990. Forschungsbericht* 16 Technische Universität Wien, Institut für Hydraulik, Gewässerkunde und Wasserwirtschaft, Wien.

Botz, R.W. and **Von der Borch, C.C.** (1984) Stable isotope study of carbonate sediments from the Coorong region, South Australia. *Sedimentology*, **31**, 837–849.

Botz, R., **Faber, E.**, **Whiticar, M.J.** and **Mrooks, J.M.** (1988) Authigenic carbonates in sediments from the Gulf of Mexico. *Earth Planet. Sci. Lett.*, **88**, 263–272.

Bristow, T.F., **Kennedy, M.J.**, **Morrison, K.D.** and **Mrofka, D.D.** (2012) The influence of authigenic clay formation on the mineralogy and stable isotopic record of lacustrine carbonates. *Geochim. Cosmochim. Acta*, **90**, 64–82.

Bronk Ramsey, C. (2009) Bayesian analysis of radiocarbon dates. *Radiocarbon*, **51**, 337–360.

Budd, D.A. (1997) Cenozoic dolomites of carbonate islands: their attributes and origin. *Earth Sci. Rev.*, **42**, 1–42.

Clayton, R.N., **Jones, B.F.** and **Berner, R.A.** (1968) Isotope studies of dolomite formation under sedimentary conditions. *Geochim. Cosmochim. Acta*, **32**, 415–432.

Deelman, J.C. (1999) Low-temperature nucleation of magnesite and dolomite. *Neues Jahrbuch für Mineralogie (Stuttgart), Monatshefte*, **7**, 289–302.

Demény, A. and **Haszpra, L.** (2002) Stable isotope compositions of CO_2 in background air and at polluted sites in Hungary. *Rapid Commun. Mass Spectrom.*, **16**, 797–804.

Draganits, E. and **Gmasz, S.** (2023) "… das sich das Wasser umb 100 Claffter lanng unnd 1½ man dieff verlorn." Ein zeitgenössischer Inspektionsbericht über den Wasserrückgang des Neusiedler Sees im Jahre 1568. *Neusiedler Jahrbuch*, **24**, 5–36.

Draganits, E., **Zámolyi, A.**, **Gier, S.**, **Hodits, B.**, **Exner, U.**, **Janda, C.** and **Grasemann, B.** (2007) Neusiedlersee/Fertő Tó area (Austria/Hungary): minimum estimates of former

lake levels. European Geosciences Union General Assembly 2007, Vienna, 15–20 April. *Geophysical Research Abstracts*, **9**, 10052.

Draganits, E., **Zámolyi, A.**, **Székely, B.**, **Timár, G.** and **Molnár, G.** (2008) Reconstruction of the Neusiedlersee (Austria/Hungary) based on historical topographic maps from 1507 to present. European Geosciences Union General Assembly 2008, Vienna, 13–18 April. *Geophysical Research Abstracts*, **10**, A-08644.

Draganits, E., **Weissl, M.**, **Zámolyi, A.** and **Doneus, M.** (2022) Lake Neusiedl area: A particular landscape at the boundary between Alps and Pannonian Basin. In: *Landscapes and Landforms of Austria: World Geomorphological Landscapes* (Ed. Embleton-Hamann, C.), pp. 207–222. Springer, Cham.

Eugster, H.P. and **Hardie, L.A.** (1978) Saline lakes. In: *Lakes, Chemistry, Geology, Physics* (Ed. Lerman, A.), pp. 237–293. Springer-Verlag, New York, N.Y.

Fally, J. and Kárpáti, L. (Eds) (2012) *Nationalpark Neusiedler See – Seewinkel. Fertő–Hanság Nemzeti Park. Monographische Studien über das Gebiet Neusiedler See und Hanság*. Nationalparkverwaltung Fertő–Hanság, Szaktudás Kiadó Ház AG, Budapest.

Fang, Y., **Hobbs, F.**, **Yang, Y.** and **Xu, H.** (2023) Dissolved silica-driven dolomite precipitation in the Great Salt Lake, Utah, and its implication for dolomite formation environments. *Sedimentology*, **70**, 1328–1347.

Federal Environment Agency Austria. (2000–2021) Online database. Available at: https://wasser.umweltbundesamt.at/h2odb/fivestep/abfrageQdPublic.xhtml.

Fenter, P., **Zhang, Z.**, **Park, C.**, **Sturchio, N.C.**, **Hu, X.M.** and **Higgins, S.R.** (2007) Structure and reactivity of the dolomite (104)-water interface: New insights into the dolomite problem. *Geochim. Cosmochim. Acta*, **71**, 566–579.

Förstner, U. (1973a) Petrographische und geochemische Untersuchungen an afghanischen Endseen. *Neues Jb. Mineral. Abh.*, **118**, 268–312.

Förstner, U. (1973b) Hydrochemische Entwicklungen in Flüssen und Seen Afghanistans. *Chem. Erde*, **32**, 216–238.

Fuchs, R. and **Schreiber, O.S.** (1985) Das Pannonien im östlichen Burgenland (Seewinkel). In: *M6 Pannonien (Slavonien und Serbien). Chronostratigraphie und Neostratotypen, Miozän der Zentralen Paratethys* (Ed. Papp, A.), pp. 68–72. Akadémiai Kiadó, Budapest.

Füchtbauer, H. and **Goldschmidt, H.** (1966) Beziehungen zwischen Calzium-Gehalt und Bildungsbedingungen der Dolomite. *Geologische Rundschau*, **55**, 29–40.

Fussmann, D., **von Hoyningen-Huene, A.J.E.**, **Reimer, A.**, **Schneider, D.**, **Babková, H.**, **Peticzka, R.**, **Maier, A.**, **Arp, G.**, **Daniel, R.** and **Meister, P.** (2020) Authigenic formation of Ca–Mg carbonates in the shallow alkaline Lake Neusiedl, Austria. *Biogeosciences*, **17**, 2085–2106.

Gaines, A.M. (1977) Protodolomite redefined. *J. Sed. Petrol.*, **47**, 543–546.

Gierlowski-Kordesch, E.H. (2010) Lacustrine carbonates. In: *Carbonates in Continental Settings: Facies, Environments, Processes* (Eds Alonso-Zarza, A.M. and Tanner, L.H.), *Dev. Sedimentol*, **61**, 1–101.

Godwin, H. (1962) Radiocarbon dating, fifth international conference. *Nature*, **195**, 943–945.

Goldsmith, J.R. and **Graf, D.L.** (1958) Relation between lattice constants and composition of the Ca-Mg carbonates. *Am. Mineral.*, **43**, 84–101.

Graf, D.L. and **Goldsmith, J.R.** (1956) Some hydrothermal syntheses of dolomite and protodolomite. *J. Geol.*, **64**, 173–186.

Gregg, J.M., **Bish, D.L.**, **Kaczmarek, S.E.** and **Machel, H.G.** (2015) Mineralogy, nucleation and growth of dolomite in the laboratory and sedimentary environment: a review. *Sedimentology*, **62**, 1749–1769.

Gunatilaka, A. (1990) Palaeolimnology of Neusiedlersee, Austria. II. The distribution of nutrients and trace metals. Hydrobiologia 214. In: *Environmental History and Paleolimnology* (Eds Smith, J.P., Appleby, P.G., Battarbee, R.W., Dearing, J.A., Flower, R., Haworth, E.Y., Oldfield, F. and O'Sullivan, P.E.), Vol. **214**, pp. 239–244. Kluwer Academic Publishers, Kluwer.

Hardie, L.A. (1987) Dolomitization; a critical view of some current views. *J. Sediment. Res.*, **57**, 166–183.

Häusler, H., **Kovács, G.**, **Wild, E.M.**, **Steier, P.** and **Heil, B.** (2021a) The Osli Formation – a Holocene lithostratigraphic unit in the Danube/Kisalföld Basin, eastern Austria and northwestern Hungary. *Aust J Earth Sci.*, **114**, 69–87.

Häusler, H., **Wild, E.M.** and **Steier, P.** (2021b) Alter und Fazies der quartären Ablagerungen in der Umgebung des Neusiedler Sees (Nördliches Burgenland, Österreich). *J. Geol. B.-A.*, **161**, 5–28.

Heine, E., **Kogelbauer, I.**, **Prokop, A.** and **Loiskandl, W.** (2014) Hydrographic surveying of the Steppe Lake Neusiedl – Mapping the lake bed topography and the mud layer. *Photogram Fernerkundung Geoinform*, **5**, 339–350.

Heine, E., **Loiskandl, W.**, **Briese, C.**, **Eberhöfer, C.** and **Csaplovics, E.** (2016) Hydrografische vermessung des neusiedler sees. *Vermessung Geoinform*, **1**, 9–24.

Heiri, O., **Koinig, K.A.**, **Spötl, C.**, **Barrett, S.**, **Brauer, A.**, **Drescher-Schneider, R.**, **Gaar, D.**, **Ivy-Ochs, S.**, **Kerschner, H.**, **Luetscher, M.**, **Moran, A.**, **Nicolussi, K.**, **Preusser, F.**, **Schmidt, R.**, **Schoeneich, P.**, **Schwörer, C.**, **Sprafke, T.**, **Terhorst, B.** and **Tinner, W.** (2014) Palaeoclimate records 60-8 ka in the Austrian and Swiss Alps and their forelands. *Quatern Sci. Rev.*, **106**, 186–205.

Herzig, A. (2014) Der Neusiedler See – Limnologie eines Steppensees. In: *Süßwasserwelten. Limnologische Forschung in Österreich* (Ed. Wöss, E.), *Kataloge des Oberösterreichischen Landesmuseums – Neue Serie*, **163**, 101–114.

Higgins, S.R. and **Hu, X.** (2005) Self-limiting growth on dolomite: Experimental observations with in situ atomic force microscopy. *Geochim. Cosmochim. Acta*, **69**, 2085–2094.

Hofbauer, B., **Viehmann, S.**, **Gier, S.**, **Bernasconi, S.M.** and **Meister, P.** (2021) Microfacies and C/O-isotopes in lacustrine dolomites reflect variable environmental conditions in the Germanic Basin (Arnstadt Formation, Upper Triassic). *Austrian J. Earth Sci.*, **114**, 66–87.

Hollander, D.J. and **McKenzie, J.A.** (1991) CO_2 control on carbon isotope fractionation during aqueous photosynthesis: a paleo pCO_2 barometer. *Geology*, **19**, 929–932.

Hsü, K.J. and **McKenzie, J.A.** (1985) Swiss lakes as a geological laboratory. Part II: Varves. *Naturwissenschaften*, **72**, 365–371.

Hua, Q., **Turnbull, J.C.**, **Santos, G.M.**, **Rakowski, A.Z.**, **Ancapichún, S.**, **De Pol-Holz, R.**, **Hammer, S.**, **Lehman, S.J.**, **Levin, I.**, **Miller, J.B.**, **Palmer, J.G.** and **Turney, C.S.M.** (2022) Atmospheric radiocarbon for the period 1950–2019. *Radiocarbon*, **64**, 723–745.

Irlweck, K., **Netrwal, C.**, **Khademi, B.**, **Spatzierer, G.** and **Feurer, K.** (1990) Ermittlung des Fortschrittes der längerfristigen Seeverlandung des Neusiedler Sees durch Bestimmung der Sedimentationsraten mittels radiochemischer Methoden. *Wissenschaftliche Arbeiten aus dem Burgenland*, **82**, 179–219.

Ivy-Ochs, S., **Monegato, G.** and **Reitner, J.** (2022) The Alps: glacial landforms from the Last Glacial Maximum. In: *European Glacial Landscapes* (Eds Palacios, D., Hughes, P.D., Garcia-Ruiz, J.M. and Andres, N.), pp. 449–460. Elsevier, Amsterdam.

Johnson, W.J. and **Goldstein, R.H.** (1993) Cambrian sea water preserved as inclusions in marine low-magnesium calcite cement. *Nature*, **362**, 335–337.

Kell-Duivestein, I.J., **Baldermann, A.**, **Mavromatis, V.** and **Dietzel, M.** (2019) Controls of temperature, alkalinity and calcium carbonate reactant on the evolution of dolomite and magnesite stoichiometry and dolomite cation ordering degree – an experimental approach. *Chem. Geol.*, **529**, 119292.

Kim, S.-T. and **O'Neil, J.R.** (1997) Equilibrium and nonequilibrium oxygen isotope effects in synthetic carbonates. *Geochim. Cosmochim. Acta*, **61**, 3461–3475.

Knie, K. (1959) Über den Chemismus der Wässer im Seewinkel und des Neusiedlersees. In: *Landschaft Neusiedlersee: Grundriss der Naturgeschichte des Großraumes Neusiedlersee Anläßlich des XIV. Internationalen Limnologen-Kongresses in Österreich 1959* (Ed. Sauerzopf, F.), *Wissenschaftliche Arbeiten aus dem Burgenland*, **23**, 65–68.

Kovács, R. (2010) Árvízvédelmi célú műszaki beavatkozások történeti áttekintése a Fertő-tavon. *A Magyar Hidrológiai Társaság*, XXVIII, Országos Vándorgyűlése, Sopron, 2010, július 7–9. Avaialble at: https://library.hungaricana.hu/hu/view/HidrologiaiVandorgyules_2010_28/?query=1956&pg=1446.

Krachler, R., **Krachler, R.**, **Milleret, E.** and **Wesner, W.** (2000) Limnochemische Untersuchungen zur aktuellen Situation der Salzlacken im Burgenländischen Seewinkel. *Burgenländische Heimatblätter*, **62**(1/2), 3–49.

Kromp-Kolb, H., **Eitzinger, J.**, **Kubu, G.**, **Fromayer, H.**, **Haas, P.** and **Gerersdorfer, T.** (2005) *Auswirkungen einer Klimaänderung auf den Wasserhaushalt des Neusiedler Sees. Forschungsprojekt im Auftrag des Amtes der Burgenländischen Landesregierung Landeswasserbaubezirksamt Schützen am Gebirge*. Endbericht. Universität für Bodenkultur, Wien. Available at: https://meteo.boku.ac.at/report/boku-met_report_01_online.pdf.

Land, L.S. (1998) Failure to precipitate dolomite at 25°C from dilute solution despite 1000-fold oversaturation after 32 years. *Aquat. Geochem.*, **4**, 361–368.

Last, W.M. (1990) Lacustrine Dolomite – an overview of modern, Holocene, and Pleistocene occurrences. *Earth Sci. Rev.*, **27**, 221–263.

Last, F.M., **Last, W.M.** and **Halden, N.M.** (2010) Carbonate microbialites and hardgrounds from Manito Lake, an alkaline, hypersaline lake in the northern Great Plains of Canada. *Sed. Geol.*, **225**, 34–49.

Last, F.M., **Last, W.M.** and **Halden, N.M.** (2012) Modern and late Holocene dolomite formation: Manito Lake, Saskatchewan, Canada. *Sed. Geol.*, **281**, 222–237.

Libby, W.F., **Anderson, E.C.** and **Arnold, J.R.** (1949) Age determination by radiocarbon content: world-wide assay of natural radiocarbon. *Science*, **109**, 227–228.

Löffler, H. (1979) Neusiedlersee: The limnology of a shallow lake in central Europe. In: *Monographiae Biologicae*, Vol. **37**. W. Junk Publishers, The Hague, 543 pp.

Lippmann, F. (1973) The system $CaCO_3$–$MgCO_3$. In: *Sedimentary Carbonate Minerals. Minerals, Rocks and Inorganic Materials, vol. 6*, pp. 148–190. Springer, Berlin, Heidelberg.

Loisl, J., **Tari, G.**, **Draganits, E.**, **Zámolyi, A.** and **Gjerazi, I.** (2017) High-resolution seismic reflection data acquisition and interpretation, Lake Neusiedl, Austria, northwest Pannonian Basin. *Interpretation*, **6**, SB77–SB97.

Lumsden, D.N. and **Chimahusky, J.S.** (1980) Relationship between dolomite nonstiochiometry and carbonate facies parameters. In: *Concepts and Models of Dolomitization* (Eds Zenger, D.H., Dunham, J.B. and Ethingtom, R.A.), *SEPM Spec Publ*, **28**, 123–137.

Machel, H.G. (2004) Concepts and models of dolomitization: a critical reappraisal. *Geol. Soc. Lond. Spec. Publ.*, **235**, 7–63.

Major, I., **Haszpra, L.**, **Rinyu, L.**, **Futó, I.**, **Bihari, Á.**, **Hammer, S.**, **Timothy Jull, A.J.** and **Molnár, M.** (2018) Temporal variation of atmospheric fossil and modern CO_2 excess at a central European rural tower station between 2008 and 2014. *Radiocarbon*, **60**, 1285–1299.

McCormack, J., **Bonttognali, T.R.R.**, **Immenhauser, A.** and **Kwiecien, O.** (2018) Controls on cyclic formation of Quaternary early diagenetic dolomite. *Geophys. Res. Lett.*, **45**, 3625–3633.

McKenzie, J.A. (1981) Holocene dolomitzation of calcium carbonate sediments from the coastal sabkhas of Abu Dhabi, U.A.E. *J. Geol.*, **89**, 185–198.

McKenzie, J.A. and **Hollander, D.J.** (1993) Oxygen-isotope record in recent carbonate sediments from Lake Greifen, Switzerland (1750-1986): application of continental isotopic indicator for evaluation of changes in climate and atmospheric circulation patterns. In: *Climate Change in Continental Isotopic Records, Vol. 78* (Eds Swart, P.K., Lohmann, K.C., McKenzie, J.A. and Savin, S.) (1993) , pp. 101–111. AGU, Washington DC.

Meister, P. and **Frisia, S.** (2019) Dolomite formation by nano-crystal aggregation in the Dolomia Principale of the Brenta Dolomites (Northern Italy). *Rivista Italiana di Paleontologia e Stratigrafia*, **125**, 183–196.

Meister, P. and **Reyes, C.** (2019) The carbon-isotope record of the sub-seafloor biosphere. In: *Tracking the Deep Biosphere through Time* (Eds Drake, H., Ivarsson, M. and Heim, C.), *Geosciences*, **507**, 1–25.

Meister, P., **Reyes, C.**, **Beaumont, W.**, **Rincon, M.**, **Collins, L.**, **Berelson, W.**, **Stott, L.**, **Corsetti, F.** and **Nealson, K.H.** (2011a) Calcium and magnesium-limited dolomite precipitation at Deep Springs Lake, California. *Sedimentology*, **58**, 1819–1830.

Meister, P., **Johnson, O.**, **Corsetti, F.** and **Nealson, K.H.** (2011b) Magnesium inhibition controls spherical carbonate precipitation in ultrabasic springwater (Cedars, California) and culture experiments. In: *Advances in Stromatolite Geobiology* (Eds Reitner, J., Quéric, N.-V. and Arp, G.), pp. 101–121. Springer-Verlag, Berlin/Heidelberg.

Meister, P., **Frisia, S.**, **Dódony, I.**, **Pekker, P.**, **Molnár, Z.**, **Neuhuber, S.**, **Gier, S.**, **Kovács, I.**, **Demény, A.** and **Pósfai, M.** (2023) Nanoscale pathway of modern dolomite formation in a shallow, alkaline lake. *Crystal Growth Design*, **23**, 3202–3212.

Middelburg, J.J., **Soetaert, K.** and **Herman, P.M.J.** (1997) Empirical relationships for use in global diagenetic models. *Deep-Sea Research I*, **44**, 327–344.

Molnár, Z., **Pekker, P.**, **Dódony, I.** and **Pósfai, M.** (2021) Clay minerals affect calcium (magnesium) carbonate precipitation and aging. *Earth Planet. Sci. Lett.*, **567**, 116971.

Mook, W.G., **Bommerson, J.C.** and **Staverman, W.H.** (1974) Carbon isotope fractionation between dissolved bicarbonate and gaseous carbon dioxide. *Earth Planet. Sci. Letters*, **22**, 169–176.

Moser, I. (1866) Der abgetrocknete Boden des Neusiedler Sees. *Jahrbuch der Geologischen Bundesanstalt*, **16**, 338–344.

Müller, G. (1970) High-Magnesian calcite and protodolomite in Lake Balaton (Hungary) sediments. *Nature*, **226**, 749–750.

Müller, G., **Irion, G.** and **Förstner, U.** (1972) Formation and diagenesis of inorganic Ca-Mg carbonates in the lacustrine environment. *Naturwissenschaften*, **59**, 158–164.

Nordeng, S.H. and **Sibley, D.F.** (1994) Dolomite stoichiometry and Ostwald's step rule. *Geochim. Cosmochim. Acta*, **58**, 191–196.

Nyirö-Kósa, I., **Rostási, Á.**, **Bereczk-Tompa, É.**, **Corab, I.**, **Koblar, M.**, **Kovács, A.** and **Pósfai, M.** (2018) Nucleation and growth of Mg-bearing calcite in a shallow, calcareous lake. *Earth Planet. Sci. Lett.*, **496**, 20–28.

O'Leary, M.H. (1981) Carbon isotope fractionation in plants. *Phytochemistry*, **20**, 553–567.

Ostwald, W. (1897) Studien über die Bildung und Umwandlung fester Körper. 1. Abhandlung: Übersättigung und Überkaltung. *Int. J. Res. Phys. Chem. Chem. Phys.*, **22**, 289–330.

Padisák, J. and **Dokulil, M.** (1994) Meroplankton dynamics in a saline, turbulent, turbid shallow lake (Neusiedlersee, Austria and Hungary). *Hydrobiologia*, **289**, 23–42.

Pascher, G.A., **Herrmann, P.**, **Mandl, G.W.**, **Matura, A.**, **Nowotny, A.**, **Pahr, A.** and **Schnabel, W.** (1999) *Geologische Karte des Burgenlandes 1:200.000*. Geologische Bundesanstalt, Wien.

Peterson, M.N.A., **Bien, C.S.** and **Berner, R.A.** (1963) Radiocarbon studies of recent dolomite from Deep Spring Lake, California. *J. Geophys. Res.*, **68**, 6493–6505.

Pina, C.M., **Pimentel, C.** and **Crespo, A.** (2022) The dolomite problem: a matter of time. *ACS Earth Space Chem.*, **6**, 1468–1471.

Preisinger, A. (1979) Limnology of a Shallow Lake in Central Europe. *Monograph Biol*, **37**, 131–138.

Preto, N., **Breda, A.**, **Corso, J.D.**, **Spotl, C.**, **Zorzi, F.** and **Frisia, S.** (2015) Primary dolomite in the Late Triassic Travenanzes Formation, dolomites, Northern Italy: facies control and possible bacterial influence. *Sedimentology*, **62**, 697–716.

Purgstaller, B., **Mavromatis, V.**, **Immenhauser, A.** and **Dietzel, M.** (2016) Transformation of Mg-bearing amorphous calcium carbonate to Mg-calcite – In situ monitoring. *Geochim. Cosmochim. Acta*, **174**, 180–195.

Rank, D., **Whylidal, S.**, **Heiss, G.**, **Papesch, W.** and **Schott, K.** (2016) Arsenal environmental-isotope laboratories 1964-2010 – more than 45 years production/application/interpretation of basic isotope-hydrological data for Central Europe. *Austrian J. Earth Sci.*, **109**, 4–28.

Reimer, P.J., **Brown, T.A.** and **Reimer, R.W.** (2004) Discussion: reporting and calibration of post-bomb ^{14}C data. *Radiocarbon*, **46**, 1299–1304.

Reimer, P.J., **Austin, W.E.N.**, **Bard, E.**, **Bayliss, A.**, **Blackwell, P.G.**, **Bronk Ramsey, C.**, **Butzin, M.**, **Cheng, H.**, **Edwards, R.L.**, **Friedrich, M.**, **Grootes, P.M.**, **Guilderson, T.P.**, **Hajdas, I.**, **Heaton, T.J.**, **Hogg, A.G.**, **Hughen, K.A.**, **Kromer, B.**, **Manning, S.W.**, **Muscheler, R.**, **Palmer, J.G.**, **Pearson, C.**, **van der Plicht, J.**, **Reimer, R.W.**, **Richards, D.A.**, **Scott, E.M.**, **Southon, J.R.**, **Turney, C.S.M.**, **Wacker, L.**, **Adolphi, F.**, **Büntgen, U.**, **Capano, M.**, **Fahrni, S.M.**, **Fogtmann-Schulz, A.**, **Friedrich, R.**, **Köhler, P.**, **Kudsk, S.**, **Miyake, F.**, **Olsen, J.**, **Reinig, F.**, **Sakamoto, M.**, **Sookdeo, A.** and **Talamo, S.** (2020) The IntCal20 northern hemisphere radiocarbon age calibration curve (0–55 CAL kBP). *Radiocarbon*, **62**, 725–757.

Reinhardt, L. and **Ricken, W.** (2000) The stratigraphic and geochemical record of playa cycles: monitoring a Pangaean monsoon-like system (Triassic, Middle Keuper, S. Germany). *Palaeogeograp. Palaeoclimatol. Palaeoecol.*, **161**, 205–227.

Reitinger, J., **Schmalfuss, R.** and **Mahler, H.** (1991) Aspekte zum Wasserhaushalt des Neusiedler Sees. *Biologisches Forschungsinstitut für das Burgenland - Bericht*, **77**, 101–107.

Rieder, M., **Wegner, W.**, **Horschinegg, M.**, **Klackl, S.**, **Preto, N.**, **Breda, A.**, **Gier, S.**, **Klötzli, U.**, **Bernasconi, S.M.**, **Arp, G.** and **Meister, P.** (2019) Precipitation of dolomite from seawater on a Carnian coastal plain (Dolomites, northern Italy): evidence from carbonate petrography and Sr isotopes. *Solid Earth*, **10**, 1243–1267.

Rodriguez-Blanco, J.D., **Shaw, S.**, **Bots, P.**, **Roncal-Herrero, T.** and **Benning, L.G.** (2012) The role of pH and Mg on the stability and crystallization of amorphous calcium carbonate. *J. Alloys Comp.*, **536**, 477–479.

Rodriguez-Blanco, J.D., **Shaw, S.** and **Benning, L.G.** (2015) A route for the direct crystallization of dolomite. *Am. Mineral.*, **100**, 1172–1181.

Sailer, C.L. and **Maracek, K.** (2019) Der Neusiedler See – ein Überblick. *Österr. Wasser- Abfallw.*, **71**, 483–493.

Sandberg, P.A. (1983) An oscillating trend in Phanerozoic non-skeletal carbonate mineralogy. *Nature*, **305**, 19–22.

Sauerzopf, F. (1959) Die Wasserstandsschwankungen des Sees. In: *Landschaft Neusiedlersee: Grundriss der Naturgeschichte des Großraumes Neusiedlersee Anläßlich des XIV. Internationalen Limnologen-Kongresses in Österreich 1959* (Ed. Sauerzopf, F.), *Wissenschaftliche Arbeiten aus dem Burgenland*, **23**, 92–101.

Schnedlitz, T. (2020) *Elemental and isotope distribution of Lake Neusiedl – elemental cycles, sources and sinks*. Unpubl. MSc Thesis, 113 p. Graz University of Technology, Graz.

Schroll, E. and **Wieden, P.** (1960) Eine rezente Bildung von Dolomit im Schlamm des Neusiedler Sees. *Tschermaks Mineralogische und Petrographische Mitteilungen*, **3**, 286–289.

Sibley, D.F., **Nordeng, S.H.** and **Barkowski, M.L.** (1994) Dolomitization kinetics in hydrothermal bombs and natural settings. *J. Sediment. Research*, **64A**, 630–637.

Soja, G., **Züger, J.**, **Knoflacher, M.**, **Kinner, P.** and **Soja, A.M.** (2013) Climate impacts on water balance of a shallow steppe lake in Eastern Austria (Lake Neusiedl). *J. Hydrol.*, **480**, 115–124.

Spötl, C. and **Vennemann, T.** (2003) Continuous-flow isotope ratio mass spectrometric analysis of carbonate minerals. *Rapid Commun. Mass Spectrom.*, **17**, 1004–1006.

Steier, P., **Liebl, J.**, **Kutschera, W.**, **Wild, E.M.** and **Golser, R.** (2017) Preparation methods of μg carbon samples for ^{14}C measurements. *Radiocarbon*, **59**, 803–814.

Stuiver, M. and **Polach, H.A.** (1977) Discussions reporting of ^{14}C data. *Radiocarbon*, **19**, 355–363.

Šujan, M., **Rybár, S.**, **Kováč, M.**, **Bielik, M.**, **Majcin, D.**, **Minár, J.**, **Plašienka, D.**, **Nováková, P.** and **Kotulová, J.** (2021) The polyphase rifting and inversion of the Danube Basin revised. *Global Planet. Change*, **196**, 103375.

Székely, B., **Zámolyi, A.**, **Draganits, E.** and **Briese, C.** (2009) Geomorphic expression of neotectonic activity in a low relief area in an Airborne Laser Scanning DTM: a case study of the Little Hungarian Plain (Pannonian basin). *Tectonophysics*, **474**, 353–366.

Talbot, M.R. (1990) A review of the palaeohydrological interpretation of carbon and oxygen isotopic ratios in primary lacustrine carbonates. *Chem. Geol.*, **80**, 261–279.

Tanner, C.B. and **Jackson, M.L.** (1948) Nomographs for sedimentation times of soil particles under gravity or centrifugal acceleration. *J. Soil Sci. Soc. Am.*, **12**, 60–65.

Tanzberger, A. (2005) *Die "Kochbrunnen" des Neusiedlersees. Ein kurzer Überblick über neue Untersuchungen*. Unpublished B.Sc. Thesis. University of Vienna, Vienna.

Tauber, A.F. (1959) Geologische Stratigraphie und Geschichte des Neusiedlerseegebietes. *Wissenschaftliche Arbeiten aus dem Burgenland*, **23**, 18–24.

Tchaikovsky, A., **Häusler, H.**, **Kralik, M.**, **Zitek, A.**, **Irrgeher, J.** and **Prohaska, T.** (2019) Analysis of $n(^{87}Sr)/n(^{86}Sr)$, $\delta^{88}Sr/^{86}Sr_{SRM987}$ and elemental pattern to characterise groundwater and recharge of saline ponds in a clastic aquifer in East Austria. *Isotopes Environ. Health Stud.*, **55**, 179–198.

Teal, C.S., **Mazzullo, S.J.** and **Bischoff, W.D.** (2000) Dolomitization of Holocene shallow-marine deposits mediated by sulfate reduction and methanogenesis in normal salinity seawater, northern Belize. *J. Sediment. Res.*, **70**, 649–663.

Teranes, J.L. and **Bernasconi, S.M.** (2005) Factors controlling $\delta^{13}C$ values of sedimentary carbon in hypertrophic Baldeggersee, Switzerland, and implications for interpreting isotope excursions in lake sedimentary records. *Limnol. Oceanogr.*, **50**, 914–922.

Teranes, J.L., **McKenzie, J.A.**, **Lotter, A.F.** and **Sturm, M.** (1999) Stable isotope response to lake eutrophication: calibration of a high-resolution lacustrine sequence from Baldeggersee, Switzerland. *Limnol. Oceanogr.*, **44**, 320–333.

Troilier, M., **White, J.W.C.**, **Tans, P.P.**, **Masarie, K.A.** and **Gemery, P.A.** (1996) Monitoring the isotopic composition of atmospheric CO2: Measurements from the NOAA global air sampling network. *J. Geophys. Res.*, **101**, 25897–25916.

Tucker, M.E. (2001) *Sedimentary petrology: an introduction to the origin of sedimentary rocks*, 3nd edn, p. 262. Blackwell, Oxford.

Vasconcelos, C., **McKenzie, J.A.**, **Bernasconi, S.**, **Grujic, D.** and **Tien, A.J.** (1995) Microbial mediation as a possible mechanism for natural dolomite formation at low temperatures. *Nature*, **377**, 220–222.

Viehmann, S., **Reitner, J.**, **Tepe, N.**, **Hohl, S.V.**, **Van Kranendonk, M.**, **Hofmann, T.**, **Koeberl, C.** and **Meister, P.** (2020) Carbonates and cherts as archives of seawater chemistry and habitability on a carbonate platform 3.35 Ga ago: Insights from Sm/Nd dating and trace element analysis from the Strelley Pool Formation, Western Australia. *Precambrian Res.*, **344**, 105742.

Von der Borch, C.C., **Lock, D.E.** and **Schwebel, D.** (1975) Groundwater formation of dolomite in the Coorong region of South Australia. *Geology*, **3**, 283–285.

Warren, J. (1990) Sedimentology and mineralogy of dolomitic Coorong Lakes, South Australia. *J. Sediment. Petrol.*, **60**, 843–858.

Warren, J. (2010) Evaporites through time: Tectonic, climatic and eustatic controls in marine and nonmarine deposits. *Earth-Sci. Rev.*, **98**, 217–268.

Wenk, H.-R., **Hu, M.** and **Frisia, S.** (1993) Partially disordered dolomite: Microstructural characterization of Abu Dhabi sabkha carbonates. *Am. Mineral.*, **78**, 769–774.

Wieden, P. (1959) Sedimentpetrographische Untersuchungen des Schlammes vom Neusiedler See (Bgld.). *Wissenschaftliche Arbeiten aus dem Burgenland*, **23**, 73–80.

Wolfram, G., **Blaschke, A.P.**, **Hainz, R.**, **Riedler, P.** and **Zessner, M.** (2021) Chemische und gewässerökologische Auswirkungen einer Dotation des Grundwassers im burgenländischen Seewinkel sowie des Neusiedler Sees mit Wasser aus der Moson-Donau. Gutachten im Auftrag des Amts der Burgenländischen Landesregierung, Abt. 5, Berichts-Nr. 20/060-B01, 106 pp., Baudirektion, Wien.

Zámolyi, A., **Salcher, B.**, **Draganits, E.**, **Exner, U.**, **Wagreich, M.**, **Harzhauser, M.**, **Gier, S.**, **Fiebig, M.**, **Lomax, J.**, **Surányi, G.**, **Diehl, M.** and **Zámolyi, F.** (2017) Latest Pannonian and Quaternary evolution at the transition between Eastern Alps and Pannonian Basin: new insights from geophysical, sedimentological and geochronological data. *Int. J. Earth Sci.*, **106**, 1695–1721.

Zhang, F., **Xu, H.**, **Konishi, H.**, **Kemp, J.M.**, **Roden, E.E.** and **Shen, Z.** (2012) Dissolved sulfide-catalyzed precipitation of disordered dolomite: Implications for the formation mechanism of sedimentary dolomite. *Geochim. Cosmochim. Acta*, **97**, 148–165.

Manuscript received 30 June 2023; revision accepted 25 October 2023

Supporting Information

Additional information may be found in the online version of this article:

Appendix S1. Supporting material for radiocarbon ages of microcrystalline authigenic carbonate in Lake Neusiedl (Austria) suggest millennial-scale growth of Mg-calcite and protodolomite.

Table S1. Calculation of carbonate $F^{14}C$ values corrected for C from organic matter.